

An aerial photograph of a glacier system. The glacier is a mix of white and light blue, with numerous small blue ponds (supraglacial lakes) scattered across its surface. The glacier flows towards a dark brown, rocky coastline. A dark blue fjord or inlet is visible, partially filled with greenish water. The sky is a pale, hazy blue.

Impact of Ice Sheet-Climate Interactions on Greenland Ice Sheet Mass Balance: Insights from Coupled CESM2-CISM2 Simulations

Thirza Feenstra

Impact of Ice Sheet-Climate Interactions on Greenland Ice Sheet Mass Balance: Insights from Coupled CESM2-CISM2 Simulations

MSc Thesis

by

Thirza Feenstra

to obtain the degree of Master of Science
at the Delft University of Technology,
to be defended publicly on January 26th, 2024 at 14:00.

Student number: 4727983
Project duration: April, 2023 – January, 2024
Thesis committee: Dr. M. Vizcaíno, TU Delft, chair and daily supervisor
Dr. Ir. B. Wouters, TU Delft
Prof. Dr. Ir. S.C. Steele-Dunne, TU Delft, external committee member

An electronic version of this thesis is available at <http://repository.tudelft.nl/>.

On the cover: Landsat 8 satellite image shows melt-water ponding on the surface of the ice sheet in North-West Greenland, on July 30, 2019. Source: NASA

Preface

I remember being an eleven-year-old girl, standing at the foot of the Briksdalsbreen glacier in Norway. I was fascinated by the enormous amount of ice, but even more so when my parents told me where the glacier had been twenty years earlier. Ten years later, I rediscovered this fascination during my BSc thesis, where I had the chance to study ice shelves. It was then that I finally discovered how to pursue my interest in climate and climate change during my studies, and started my MSc program in Geoscience and Remote Sensing, which could not have been a better choice.

The choice to study the Greenland ice sheet, an area very sensitive to climate change, is one I do not regret. I learned a lot during the ten months of thesis work, but one thing I discovered stood out: I love doing research. Despite being confronted with the harsh reality of our changing climate, I have really enjoyed studying Greenland and the climate, which would not have been possible without Miren's help. Thanks for helping me understand a little bit more of the complexity of our planet. You always made time to frown upon graphs together a bit longer and to do our 'detective work' when we found out one of the simulations was wrong, which I really appreciate. Bert, thank you for your insights on the statistics part of my thesis, you helped me make sense of all the different options and problems. Miren, Bert and Susan, a big thanks for all the feedback along the way and for boosting my confidence as a researcher.

I look back at a great six and a half years of studying in Delft, for which I want to thank all the friends I made at Proteus, Dodeka, Snellius, the stables or anywhere else. To my roommates Annika, Klaske, Lotus and Hilde: thanks for pulling me out of the 'thesis hole' every now and then and sharing our daily lives during breakfast or dinner. Floor, the much-needed hours going cycling or running together while sharing our (thesis) ups and downs were a great way to clear my mind. To all my fellow MSc thesis students in room 3.36, I am very grateful for our time together in the 'afstudeerhok'. Our supportive atmosphere, the many shared coffee and lunch breaks and all other activities after study hours made me enjoy my time as a thesis student even more. Finally, I want to thank my parents and sister. The fact that I moved three hours away and was not always able to visit often was not always easy, but you have always supported me unconditionally.

Thirza Feenstra
Delft, January 2024

Impact of Ice Sheet-Climate Interactions on Greenland Ice Sheet Mass Balance: Insights from Coupled CESM2-CISM2 Simulations

Thirza Feenstra¹

¹Geoscience and Remote Sensing, Delft University of Technology, Delft, The Netherlands

Abstract. The Greenland Ice Sheet (GrIS), which stores freshwater equal to more than seven meters of potential sea level rise, strongly interacts with the global, Arctic and North Atlantic climate. In a warming climate, the GrIS has been losing mass and is projected to lose mass at an increasing rate. The interactions between the GrIS and the climate have the potential to amplify or dampen GrIS mass balance responses to a CO₂ forcing. We investigate the impact of ice sheet-climate interactions on the mass balance and climate of the GrIS using the Community Ice Sheet Model version 2 (CISM2) coupled to the Community Earth System Model version 2 (CESM2). We compare idealized simulations with a non-evolving and evolving ice sheet topography in which we apply an annual 1 % increase until we reach four times pre-industrial (PI) CO₂ concentrations. Furthermore, we analyze an idealized simulation in which we first apply a 4x PI CO₂ forcing and thereafter annually reduce atmospheric CO₂ by 5 % until PI concentrations are reached. By comparison of a 1- and 2-way coupled simulation, we find significant changes in atmospheric blocking, precipitation and cloud formation over Greenland as the GrIS topography evolves, acting as negative feedback mechanisms on mass loss. Besides, we find that a uniform temperature lapse rate misrepresents temperature changes in the ablation area, leading to an overestimation of the positive melt-elevation and melt-albedo feedback in 1-way coupled simulations, resulting in an overestimation of mass loss. During a 350 year 4xPI CO₂ forcing period, the ice sheet loses a total mass of 1.1 m sea level equivalent, and part of its margins retreat land inward. When applying an annual 5 % decrease in CO₂ to 1xPI CO₂ concentrations, melt reduces rapidly. The small discharge concerned with the retreated state of the ice sheet allows for halting the GrIS mass loss, despite a surface mass balance that is only slightly positive under a remaining global warming of 2 K. During a complex transitional phase towards a colder climate, the GrIS, Arctic and North Atlantic ocean strongly interact, causing the area south of the GrIS to transition from a 'warming hole' towards a 'cooling hole'. Elevated atmospheric temperatures, larger ocean heat transport and a poorer state of the snowpack, compared to the initial pre-industrial state, result in limited regrowth of the ice sheet under reintroduced PI CO₂ conditions.

1 Introduction

Over the past century, the rate of global mean sea level rise (SLR) has exceeded any previous period (Fox-Kemper et al., 2021) and has been accelerating since the late 1960s (Dangendorf et al., 2019). The Greenland ice sheet (GrIS), storing more than seven meters of potential SLR (Morlighem et al., 2017), is responsible for 18 % of contemporary SLR (Otosaka et al., 2023) and its contribution is expected to increase (Bamber et al., 2019; Goelzer et al., 2020). Besides, the sixth assessment report (AR6) of the Intergovernmental Panel on Climate Change (IPCC; Fox-Kemper et al., 2021) attributed the largest uncertainties in future sea level rise to the GrIS and the Antarctic ice sheet (AIS). Therefore, understanding the physical drivers for GrIS mass loss, as well as being able to model the GrIS mass balance is crucial to obtain reliable projections of global and regional SLR.

Contemporary climate change, which can be attributed to anthropogenic greenhouse gas emissions (Jones et al., 2013; Ribes and Terray, 2013), influences surface mass processes on GrIS as a result of rising Northern Hemisphere summer temperatures (Hanna et al., 2008). Moreover, changes in the GrIS have the potential to influence local and global climate (Vizcaíno, 2014) because of its interaction with every other component of the Earth system through various processes and feedbacks (Fyke et al., 2018, Appx. B). Important feedback mechanisms include the positive melt-elevation feedback (Edwards et al., 2014; Vizcaíno, 2014; Fyke et al., 2018), the positive melt-albedo feedback (Box et al., 2012; Fyke et al., 2018) and the negative melt-discharge feedback (Goelzer et al., 2013; Fürst et al., 2015; Vizcaíno et al., 2015). The strong coupling between the

GrIS and the atmosphere potentially influences atmospheric circulation and precipitation patterns (Ridley et al., 2005; Fyke et al., 2018). The GrIS heavily interacts with the ocean, as the North Atlantic Meridional Overturning Circulation (NAMOC) influences GrIS temperatures, while freshwater influxes as a result of GrIS mass loss can influence the strength of the NAMOC (Driesschaert et al., 2007). Accounting for these interactions between the Earth system and the GrIS in climate models is critical to obtain reliable projections of SLR and GrIS evolution (Vizcaíno, 2014; Fyke et al., 2018). It has been shown that 1-way coupled simulations, in which changes in the state of the GrIS are not communicated to the Earth system model, overestimate multi-centennial GrIS mass loss (Ridley et al., 2005; Gregory et al., 2020), as several feedbacks are not represented in these simulations. Ridley et al. (2005) identify more precipitation and less melt in a 2-way coupled simulation, in which the GrIS is an interactive component within the Earth system model, and attribute this to a change in atmospheric circulation patterns. In contrast, Gregory et al. (2020) attribute the smaller mass loss to an increase in cloud fraction, causing an increase in reflected shortwave radiation and a land inward migration of precipitation patterns as a result of the topographic changes.

Considering that by 2022, global temperatures have increased by 1.09°C (0.95 - 1.20) compared to the 1850 to 1900 baseline (Gulev et al., 2023), reaching the 1.5°C goal of the Paris Agreement has become more unlikely over time (Matthews and Wynes, 2022). The increasing global temperatures call for the investigation of 'overshoot' scenarios. Applying a temperature overshoot to the GrIS could have large implications for the evolution of the GrIS-induced SLR, as GMSL could rise substantially under the larger temperatures during an overshoot period. Consequently, investigating the response of the GrIS to these kinds of scenarios is of great importance to assess the feasibility and implications of following an overshoot pathway. Previous work (Ridley et al., 2010; Robinson et al., 2012; Gregory et al., 2020; Bochow et al., 2023) shows that temperature and volume thresholds for irreversible GrIS mass loss might exist. If temperature overshoots are limited, and the ice sheet does not lose a critical ice volume, mass loss can be halted or might even be reversible. However, not all models account for ice sheet-climate interactions and no assessment has been done on what interactions play a role in determining whether or not deglaciation rates can be reversed. As ice sheet-climate interactions could potentially accelerate or slow down the changes in GMSL caused by the response of the GrIS to CO₂ reduction, it is important to account for them to obtain a reliable projection of SLR.

With the development of a coupling (Muntjewerf et al., 2021) between the Community Earth System Model version 2 (CESM2; Danabasoglu et al., 2020) and the Community Ice Sheet Model version 2 (CISM2; Lipscomb et al., 2019), it is possible to account for the ice sheet-climate interactions resulting from a dynamically evolving ice sheet. CESM2 can produce a realistic surface mass balance (SMB) by using a surface energy balance (SEB) scheme and accounts for the interactions between the different model components. Several studies (e.g. Muntjewerf et al., 2020b; Sellevold and Vizcaíno, 2020) have analyzed coupled CESM2-CISM2 simulations, but the effect of incorporating this coupling has not yet been quantified.

In this paper, we use the coupled configuration of CESM2-CISM2 to assess the impact of ice sheet-climate interactions on the mass balance of the GrIS. We evaluate the impact of these interactions under an idealized extreme warming scenario, in which we annually increase atmospheric CO₂ by 1 % from pre-industrial (PI) concentrations until four times PI CO₂. First of all, we compare two nearly identical simulations in a 1-way and 2-way coupled configuration. Besides, we analyze an idealized 2-way coupled simulation in which we bring back PI CO₂ concentrations after 350 years, to assess the impact of ice sheet-climate interactions on the response of GrIS deglaciation rates to CO₂ reduction.

In section 2 we describe the CESM2-CISM2 model setup, the simulations conducted and our analysis methods. Section 3 assesses the influence of the coupling on the simulated GrIS mass loss, whereas section 4 gives an overview of the most important climate-ice sheet interactions that influence the GrIS mass balance. In section 5 we address the GrIS mass balance response to the reintroduction of PI CO₂ conditions and investigate the related climate-ice sheet interactions. We discuss our results and draw conclusions in sections 6 and 7 respectively.

2 Method

2.1 Model description

We use the Community Earth System Model version 2 (CESM2; Danabasoglu et al., 2020) and the Community Ice Sheet Model version 2 (CISM2; Lipscomb et al., 2019), which are coupled to account for a dynamic ice sheet. CESM2 is a state-of-the-art community-developed Earth System Model (ESM), developed by the National Center for Atmospheric Research (NCAR). CESM2 consists of different component models for land and land biochemistry, atmosphere, river runoff, surface waves, ocean and marine biochemistry, sea ice and land ice, which are coupled to exchange states and fluxes (Danabasoglu et al., 2020).

The atmosphere model is the Community Atmosphere Model version 6 (CAM6; Gettelman et al., 2019), which runs on a nominal 1° (1.25° in longitude and 0.9° in latitude) grid and has 32 vertical levels. The Community Land Model version 5 (CLM5; Lawrence et al., 2019) shares the CAM6 horizontal grid. In CLM5, every grid cell is divided into one or multiple fractions of land units, which can be glacier, lake, wetland, urban, vegetation and crop surface. The calculations are carried out separately over the different land units. The model has a fixed number of vertical layers for the soil, whereas there is a variable number of layers for snow and firn, with a maximum snow depth of 10 m water equivalent. The model allows for snow compaction into firn and eventually into ice when the snow layer exceeds the maximum snow depth of 10 water equivalent. The snow albedo is calculated with the SNOW, ICE and Aerosol Radiation Model (SNICAR; Flanner et al., 2021). The surface runoff from melt and rain is routed to the ocean using the Model for Scale Adaptive River Transport (MOSART; Li et al., 2013). Modeling the ocean is done using the Parallel Ocean Program version 2 (POP2; Smith et al., 2010). POP2 has a resolution of a nominal 1° , with a uniform resolution equal to 1.125° in the zonal direction. The sea ice model is the Los Alamos National Laboratory sea ice model version 5 (CICE5; Hunke et al., 2017). CICE5 shares the grid with POP2. The model consists of an ice thermodynamic model, an ice dynamics model and a transport model that computes both horizontal transport as well as transport in thickness space.

The GrIS is modeled using the Community Ice Sheet Model version 2 (CISM2; Lipscomb et al., 2019). CISM2 is a parallel 3D thermodynamic model, which solves the momentum balance and computes the thickness and temperature over the ice sheet (Lipscomb et al., 2019). CISM2 has a 4 km rectangular grid, with 11 vertical sigma levels. The model uses approximations of the Stokes equations for incompressible viscous flow and a pseudo-plastic sliding law to parameterize basal sliding. Floating ice at marine margins is immediately discharged to the ocean using a floating criterion (Muntjewerf et al., 2021).

2.2 Coupling description

By coupling CISM2 with CESM2, interactions and feedback mechanisms between the ice sheet and the climate are accounted for in the projected evolution of GrIS mass loss. The coupling of CISM2 is bi-directional with CLM5 and CAM6 and unidirectional with POP2 (Figure 1) and has a frequency of once per model year, except for the communication of the GrIS topography to CAM6, which is done every 5 or 10 years. In CLM5, the SMB and SEB are computed for multiple elevation classes (Sellevold et al., 2019), which allows for resolving the large heterogeneity around the steep ice sheet margins and for remapping of the SMB on the ice sheet model grid, which is done using trilinear interpolation and renormalization (Muntjewerf et al., 2021). For every elevation class, the surface energy fluxes from CLM5 are scaled down, after which their impact on the SMB can be computed. The grid cell temperature is downscaled using a uniform lapse rate of -6 K/km. Precipitation falls as snow if the elevation-corrected near-surface temperature is below -2°C and as rain if this temperature is above 0°C . Between -2°C and 0°C precipitation falls as a mix of rain and snow (Muntjewerf et al., 2021). As the ice sheet loses mass and therefore the ice sheet topography and extent evolve, the updated topography and ice sheet margins are communicated to CLM5. In CLM5, the land units and topographic height are updated according to the updated ice sheet margins and topography for all elevation classes (Muntjewerf et al., 2021). The changing ice sheet topography does not only influence the computations in CLM5 but those in CAM6 as well, as the topography influences atmospheric circulation. Therefore the ice sheet topography computed in CISM2 is communicated to CAM6, where it is remapped to the CAM6 grid in the form of surface geopotential height

120 (Muntjewerf et al., 2021). Regarding the uni-directional coupling with the ocean, CISM2 computes the annual ice discharge and basal melting, which is communicated to POP2 and then supplied to the ocean at a constant rate throughout the following year. Coupling from POP2 to CISM2 is not yet implemented in CESM2. Therefore ocean-forced melting of marine-terminating glaciers is not accounted for (Muntjewerf et al., 2021).

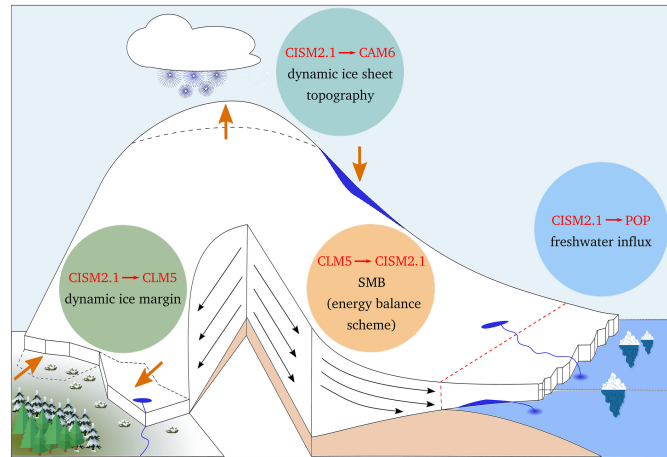


Figure 1. Schematic of four elements of coupling between ice sheets and other Earth system components, courtesy of M. Petrini (Muntjewerf et al., 2021). The land model (CLM5) receives the location of the ice sheet margin from the ice sheet model (CISM2). The land and the atmosphere (CAM6) models receive the dynamic GrIS topography from CISM2. Besides, CISM2 provides the freshwater influx to the ocean model (POP). The ice sheet model itself receives the SMB from CLM5 to compute changes in GrIS topography and extent.

2.3 Ice sheet simulations

125 In this study, we analyze both 1- and 2-way coupled simulations. The 1-way coupled simulation is a simulation in which there is no interaction between the GrIS and the climate. The climate model is forced with a constant GrIS topography in the land and the atmosphere model and the freshwater fluxes from the GrIS to the ocean model are constant. The resulting climate and SMB are downscaled using elevation classes (Sellevoold et al., 2019), using a temperature lapse rate of -6 K/km and are interpolated onto the CISM grid. This forcing results in a changing GrIS topography in CISM. However, this is not communicated to the other model components when using 1-way coupling. In contrast to the 1-way coupled run, in the 2-way coupled runs the changes in the GrIS topography and surface processes that are computed in CISM2 are communicated to the other model components every model year. This means that POP2 will receive updated freshwater fluxes and that CLM5 and CAM6 will receive an updated topography from CISM2. Therefore, topography-related feedback mechanisms will affect the state of the GrIS and the climate.

135 First of all, we compare a 1-way and a 2-way coupled simulation forced with a 4xCO₂ scenario. We apply a yearly 1 % increase in CO₂ concentration until a CO₂ concentration equal to four times the PI CO₂ concentration (1140 ppm) is obtained in year 140. After year 140, we keep the CO₂ concentration constant at 4xCO₂. The 4xCO₂ scenario is an extreme warming scenario, which after the year 140 has a similar radiative forcing as the SSP5-85 scenario by the end of the twenty-first century (Muntjewerf et al., 2020a). Besides, we analyze a 2-way coupled simulation, in which we decrease the CO₂ concentration by an annual 5 % between years 350 and 377 until PI CO₂ conditions are reached, after which the CO₂ concentration remains constant. We analyze 500 simulation years when comparing the 1- and 2-way coupled simulation and 925 simulation years of the CO₂ reduction simulation. The climate and ice sheet exchange information every year for the first 500 years of the simulation. After year 500, the climate does not change rapidly anymore. Therefore, to save computational resources, the coupling is done every 5 years after the year 500. Next to the CO₂ forcing experiments, we use a 300 year PI control simulation with a constant PI CO₂ concentration for comparison.

2.4 Definition of ice sheet and climate metrics

To assess GrIS mass loss, we use CESM2-CISM2 to compute the (surface) mass balance. The total GrIS mass balance (MB) is defined as the sum of the SMB, basal mass balance and ice discharge. The SMB can be computed by subtracting the runoff and sublimation from the precipitation over the ice sheet. Precipitation is the sum of snow and rain. Snow directly contributes positively to the SMB, while rain can either have a net SMB contribution of zero if it runs off or a positive contribution if it refreezes. Besides, melted snow and ice can also be divided into a fraction that contributes to the runoff and a fraction that refreezes. Therefore, additionally, we can express the SMB as the sum of melt and sublimation subtracted from the sum of snow and refreezing. Then, we define the refreezing capacity as the amount of refreezing divided by the amount of available water, which consists of meltwater and rainfall. The model computes the energy available for melt using the surface energy balance (SEB). The melt energy is equal to the sum of the net radiative heat flux (the sum of shortwave and longwave radiation), the turbulent heat flux (the sum of latent and sensible heat) and the ground heat flux.

Besides considering the mass and energy balances, we use several other ice sheet metrics. We compute the equilibrium line altitude (ELA) from the hypsometric curve, which represents the cumulative area distribution of the ice sheet with respect to elevation. The mean ELA is then defined as the elevation corresponding to the extent of the ablation area, which is the area with a negative SMB. We consider lapse rates to assess the effect of elevation on ice sheet surface processes. The lapse rates are computed by dividing the difference in the mean state of a variable between the 1- and 2-way simulation by the difference in the elevation between the 1- and 2-way simulation for the years 480-500. Thresholds of 250 m elevation difference and an ice sheet fraction of 90% of the grid cell are taken to exclude grid cells in which most of the changes are not caused by elevation changes. As these lapse rates describe the change in a variable resulting from elevation change, rather than the rate of change over a changing pressure level as described by the free atmospheric lapse rate, these lapse rates are not restricted by physical relationships.

We assess changes in atmospheric circulation by considering Greenland blocking events, the North Atlantic Oscillation and integrated vapor transport. The Greenland Blocking Index (GBI) is computed using the method proposed by Hanna et al. (2018), for both the summer (JJA) and winter (DJF). We subtract the area-weighted mean of the 500 hPa geopotential height over the Arctic region (60–80° N) from the Greenland region (60–80° N, 20–80° W) and normalize with respect to the control simulation. We define the North Atlantic Oscillation (NAO) index as the principle component corresponding to the leading empirical orthogonal function (EOF) of the seasonal (JJA and DJF) sea-level pressure in the North Atlantic region (20-80° N, 90° W - 40° E), normalized with respect to the control simulation (Hurrell, 1995). The integrated vapor transport (IVT) north- and eastward components are computed following Reynolds et al. (2022), using:

$$IVT = -\frac{1}{g} \int_{1000}^{300} qV dp$$

where g is gravity, q is specific humidity, V is wind velocity and p is pressure. We integrate from 1000 to 300 hPa. We compute the total IVT from the north- and eastward IVT components.

Finally, the North Atlantic Meridional Overturning Circulation (NAMOC) index is defined as the maximum strength of the overturning stream function north of 28° N and below 500 m depth and the Arctic sea ice extent is defined as the area north of 60° N where sea ice concentration is greater than 15 %.

We consider 20 data points in time for centered moving averages and periodic means to obtain a climatological mean state and variability. This means that before the year 500, 20 years are considered, whereas after the year 500, 100 years are considered. As the climate is evolving less rapidly after the year 500, a 100 year mean will be able to represent the mean state of the climate, while being consistent in terms of variability compared to the period before the year 500.

2.5 Emergence and recovery

We use the emergence concept applied by Fyke et al. (2014) to assess whether the differences between the 1- and 2-way simulations are significant. We define the first year of significant difference as the first year that the 20 year centered moving

average of the differences between the 1- and 2-way simulation has emerged from the natural variability of the differences. We define the latter as all absolute values that are smaller than one standard deviation ($1-\sigma$). The $1-\sigma$ interval is then defined as $[-\sigma_{\text{control}}\sqrt{2}, \sigma_{\text{control}}\sqrt{2}]$. σ_{control} is obtained from a 2-way coupled control simulation. We assume that this control simulation can represent the mean state of a similar 1-way control simulation, as the ice sheet is nearly in equilibrium, having a limited mean SLR rate of -0.03 mm yr^{-1} , and its variance only represents natural variability. When the 20 year centered moving average of the difference has migrated permanently outside the $1-\sigma$ interval, we consider the signal emerged.

To assess whether processes can recover to their PI state after the reintroduction of PI CO_2 levels, we apply a modified approach of the aforementioned emergence concept. A variable is considered recovered if the 20 year centered moving average returns within one standard deviation ($1-\sigma$) from the PI mean and stays within the $1-\sigma$ interval (obtained from the control simulation) for the remainder of the simulation. In case a variable has not recovered by the end of the simulation, we compute an extrapolated year of recovery from the remaining linear trend over the last 100 years (825 - 925) and the remaining anomaly of the mean state of the variable in the last 100 years of the simulation with respect to the closest boundary of the $1-\sigma$ confidence interval. Besides, we compute the relative amount of recovery, by comparing the remaining anomaly in the final 100 years of the simulation to the maximum response during the $4x\text{CO}_2$ forcing period.

3 Simulated mass loss in the 1- and 2-way coupled simulation

To assess the impact of simulating a dynamic ice sheet, we first consider differences in the global and regional climate, to see whether this affects GrIS mass loss. As a response to the CO_2 forcing (Figure 2a), global temperatures rise, with a global warming response of nearly 10 K by year 500, which is not affected by the coupling (Figure 2b). Under the $4x\text{CO}_2$ forcing, the North Atlantic Meridional Overturning Circulation (NAMOC) collapses in around 150 years in both simulations (Figure 2c). A near-zero total mass balance in the first 120 years (Figure 3a) results in limited mass loss in this period (Figure 3b). During these years, the NAMOC evolution in the 1- and 2-way coupled simulations is similar, showing that this NAMOC collapse is not strongly related to increased freshwater fluxes from the GrIS.

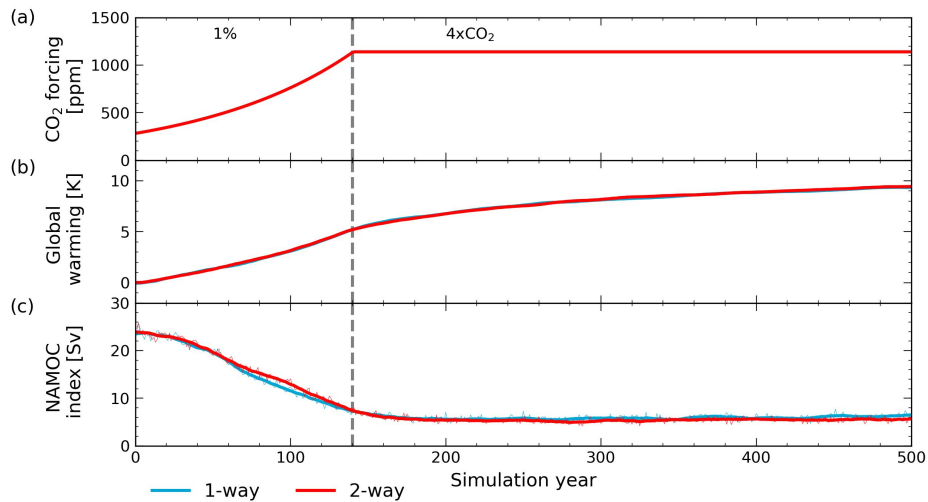


Figure 2. Evolution of 1-way (blue) and 2-way (red) coupled simulations for (a) CO_2 forcing [ppm], (b) global warming [K] and (c) NAMOC index [Sv]. The grey dashed line indicates the end of the 1 % CO_2 ramp-up period and the start of the continuous $4x\text{CO}_2$ period. None of the differences are significant.

After year 120, there is an accelerating decrease in SMB, which is strongest in the 1-way simulation (Figure 3a, Figure A1g-j), resulting in the separation of the responses in the year 282. In contrast, the contribution from ice discharge decreases in both simulations due to the melt-discharge feedback, as the ice sheet starts retreating (Figure A1b-e). Due to the small ice discharge contribution in both simulations, the total mass balance differences emerge in the same year as the SMB. During the simulation, the 1-way simulation consistently projects $17.0 \pm 0.4 \%$ more mass loss ($p < 0.01$). GrIS area loss acceleration is

215 slightly delayed compared to the mass loss with the differences becoming significant in the year 300 (Figure 3c). Ice mass is
 mainly lost in the margins, both in thickness and extent, although less strongly in the 2-way coupled simulation (Figure A1b-
 e). The increased melting of the ice sheet is represented in the heightening of the equilibrium line altitude (ELA; Figure 3d)
 and the expansion of the ablation area (the area with negative SMB; Figure 3e). As melting is stronger in the 1-way case,
 the ablation area expands faster and the ELA heightens faster. However, the ELA and extent of the ablation area of the two
 220 simulations have converged in years 320 and 400 respectively. As the GrIS loses mass, the equilibrium line moves more land
 inward, but its altitude does not increase strongly anymore, as the ice sheet's elevation decreases simultaneously. As the ice
 sheet extent becomes smaller, parts of the ablation area are lost, slowing down the increase in the total percentage of ablation
 area. The period of this slow increase is reached later in the 2-way simulation, but results in a period (year 400-464) in which
 the division in ablation and accumulation area is similar in both simulations.

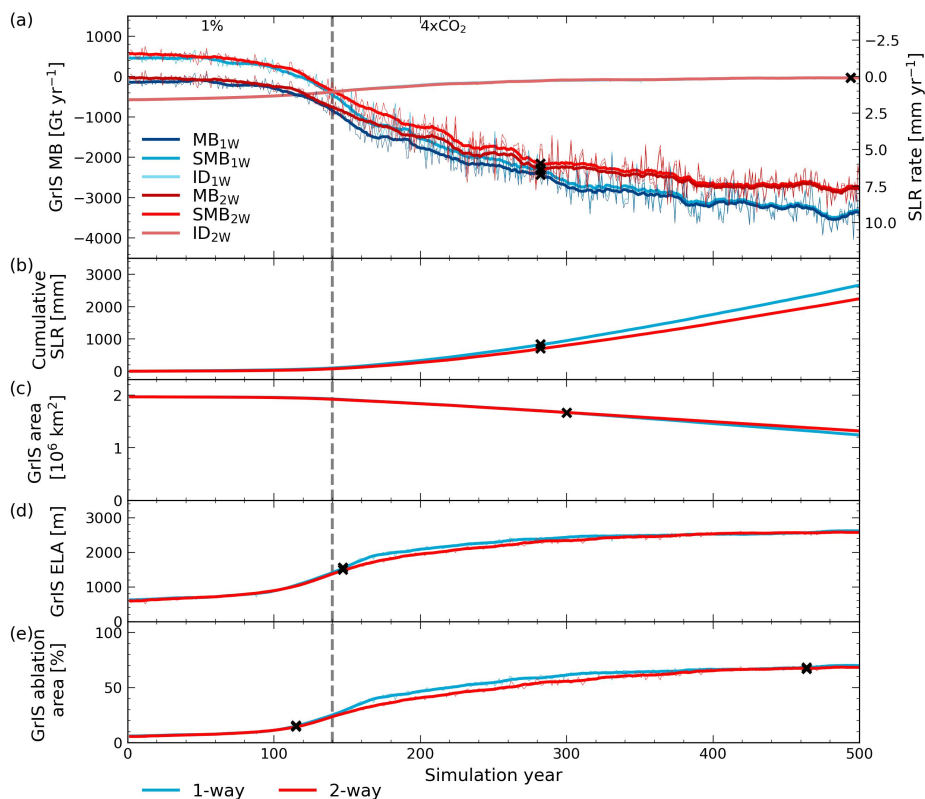


Figure 3. Evolution of 1-way (blue, 1W) and 2-way (red, 2W) coupled simulations for (a) GrIS total mass balance (MB) [Gt yr⁻¹] and its components ice discharge (ID) and surface mass balance (SMB) (the basal mass balance is not displayed as its contribution is limited), (b) GrIS induced cumulative sea level rise [mm], (c) GrIS area [10⁶ km²], (d) GrIS equilibrium line altitude [m] and (e) GrIS ablation area compared to total GrIS area [%]. The mass balance (components) in (a) can be directly converted to the GrIS-induced SLR rate [mm yr⁻¹]. The grey dashed line indicates the end of the 1 % CO₂ ramp-up period and the start of the continuous 4xCO₂ period. If the differences between the 1- and 2-way coupled simulations become significant throughout the simulation, the first year of significant difference is marked with a black cross. In (b) the year of significance for the annual SLR is given. In (d, e) the year of significant difference before the convergence between the two simulations is given as well.

225 4 Climate feedback response to a dynamic GrIS topography

The differences in the mass balance evolutions of the two simulations indicate that local climate and GrIS surface processes are affected by the coupling. We first consider the positive melt-elevation and melt-albedo feedback, which enhance mass loss, and assess their representation in the 1-way coupled configuration, as we parameterize these feedbacks in the 1-way simulation. Then, we analyze negative feedbacks, related to atmospheric processes, by considering precipitation, atmospheric circulation
 230 and clouds.

4.1 Positive feedbacks resulting from GrIS surface changes

The melt response to the CO₂ forcing results in a lowering of the topography. This enhances the melt-elevation feedback (Figure 4), as lower elevations result in higher temperatures, and consequently enhances the melt-albedo feedback, as bare ice and melting snow have a lower albedo. In the 2-way simulation, we account for this, by allowing the topography to evolve, while in the 1-way simulation, the topography is constant. The effect of incorporating a dynamic topography on the melt becomes significant in the year 215 and accounting for this results in 66 % more melt in the 2-way simulation by year 500. Since both simulations include an interactive calculation of the albedo, the melt differences include both the melt-elevation and the resulting enhancement of the melt-albedo feedback. Besides, the melt is affected by the negative atmospheric-related feedbacks as well.

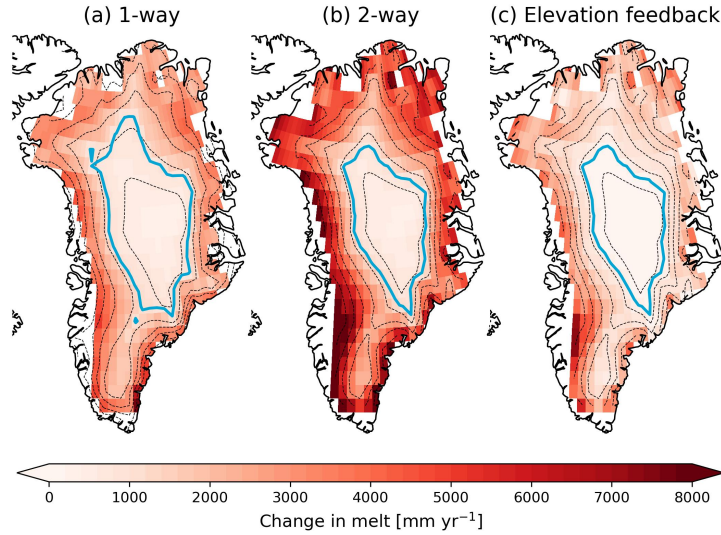


Figure 4. Change in melt [mm yr^{-1}] for years 480-500 with respect to the control simulation for the (a) 1-way and (b) 2-way coupled simulation. (c) difference between (a) and (b), showing the effect of elevation change on melt evolution. The black dashed lines depict contour lines for every 500 m elevation of (a) the 1-way and (b-c) the 2-way simulation. The light blue line represents the ELA of (a) the 1-way and (b-c) the 2-way simulation. All changes are significant.

The 2 m air temperature (T_{2m}) increase resulting from elevation changes causes changes in the GrIS surface energy fluxes. To assess the effect of the elevation change on the T_{2m} and the downwelling longwave radiation (LW_{in}), we compute lapse rates (Figure A2, Figure A3) and compare them with the applied lapse rates in the 1-way coupled simulation (Table 1). The applied lapse rate of -6 K km^{-1} corresponds relatively well to the annual mean temperature lapse rate (Table 1). However, applying these pre-defined lapse rates leads to an overestimation of the T_{2m} in summer and an underestimation in winter. The overestimation in summer is partly compensated by not applying an LW_{in} lapse rate, resulting in an underestimation of LW_{in} in the 1-way coupled simulation. In summer, the surface in the ablation area, which is the area in which most of the elevation change happens, is at the melting point (Figure A2). Therefore, part of the available energy will be used for melting instead of heating the atmosphere, leading to a limited T_{2m} increase in the ablation area. The LW_{in} lapse rates show a similar pattern, as these are largely influenced by atmospheric temperatures.

To assess the effect of the difference in applied lapse rates, we consider a point that transitions to the ablation area (66.44° N , 45° E , shown in Figure A3). Here, the 1- and 2-way simulations show a similar response as long as the elevation does not change (Figure 5). As soon as the mean summer surface temperature reaches melting point (Figure 5c) and elevation starts to lower (Figure 5a), T_{2m} and melt responses start to diverge between the simulations. Since in the 1-way simulation, the temperature and surface fluxes correspond to a fixed elevation, melt does not increase as strongly as in the 2-way case. However, adding the temperature change due to the lowering of the elevation by considering the -6 K km^{-1} lapse rate (dashed blue in Figure 5c) results in a large overestimation of the 1-way T_{2m} , potentially causing an overestimation of the sensible and latent heat flux contribution to the melt energy. Although this is partially compensated by an underestimation of the incoming

Table 1. 2 m air temperature [K km^{-1}] and downwelling longwave radiation [$\text{W m}^{-2} \text{ km}^{-1}$] lapse rates for annual, summer (June, July, August) and winter (December, January, February) means, compared to the applied lapse rates in the 1-way coupled simulation, computed using the years 480-500.

Mean lapse rate	T_{2m}	LW_{in}
Annual	-7.3 K km^{-1}	$-40.0 \text{ W m}^{-2} \text{ km}^{-1}$
Summer (JJA)	-2.4 K km^{-1}	$-22.1 \text{ W m}^{-2} \text{ km}^{-1}$
Winter (DJF)	-12.0 K km^{-1}	$-55.8 \text{ W m}^{-2} \text{ km}^{-1}$
Applied in 1-way	-6 K km^{-1}	$0 \text{ W m}^{-2} \text{ km}^{-1}$

longwave flux, this could result in an overestimation of the melt-elevation and melt-albedo feedback when computing mass loss in CISM2, which could explain part of the overestimated mass loss.

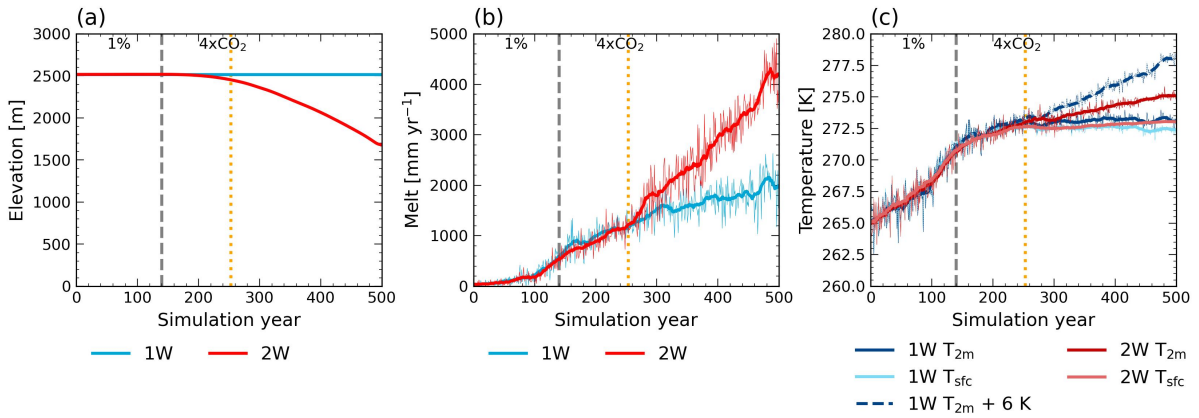


Figure 5. Evolution of (a) elevation [m], (b) annual melt [mm yr^{-1}] and (c) mean summer (June, July, August) 2 m air and surface temperature [K] for the 1-way (blue, 1W) and 2-way (red, 2W) coupled simulations for a point that transitions to the ablation area (66.44° N , 45° E , shown in Figure A3). The grey dashed line indicates the end of the 1 % CO_2 ramp-up period and the start of the continuous $4x\text{CO}_2$ period. The orange dashed line indicates the timing of reaching surface melt conditions throughout the whole summer (273 K). In (c) the blue dashed line shows the evolution of 1-way T_{2m} when applying the -6 K km^{-1} lapse rate to the 2-way elevation change.

260 4.2 Negative feedbacks resulting from local climate change

Changes in the GrIS topography can change the local climate in several ways. First of all, a lowering topography results in an overall increase in precipitation, especially in the southeast (Figure 6a). Higher temperatures in the 2-way simulation result in more evaporation from the surrounding oceans. An increase in the transport of this moisture leads to increased precipitation over the GrIS (Figure 6d). In some locations in the western and northern margins, precipitation decreases, although not significant
265 in all locations, as orographic precipitation moves more land inward, following the margin. In the western margins, we see a corresponding strong increase in IVT. The difference in precipitation is mainly caused by larger rainfall (Figure 6c), rather than larger snowfall (Figure 6b). Snowfall moves more towards the interior, as temperatures in the margins become too high for precipitation to fall as snow. As a result, snowfall decreases in the ablation area and increases in the accumulation area (Figure A4).

270 The effect of the presence of the cold and high-elevation GrIS on atmospheric circulation changes as its surface lowers and warms. The changing GrIS surface results in a large reduction of Greenland blocking (Figure 7a, b), especially in summer. This aligns with the positive relationship between orography and blocking events (Mullen, 1989; Narinesingh et al., 2020). The changing GrIS geometry has no significant effect on the phase of the NAO (Figure 7d, e). However, the summer NAO index shows a trend towards a positive phase as a result of the warming in both simulations ($p < 0.001$). The observational
275 records show a coupling between the GBI and NAO index (Davini et al., 2012). Similarly, we find a strong correlation between

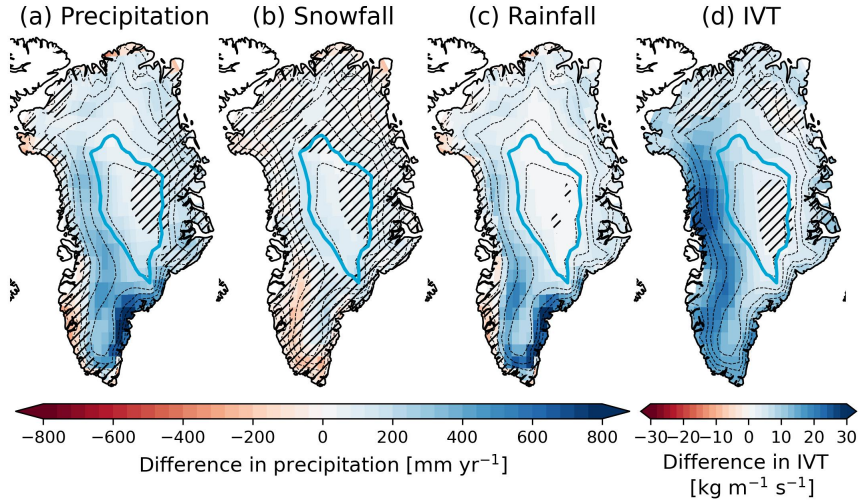


Figure 6. Annual mean differences (2-way minus 1-way) resulting from the coupling for (a) total precipitation [mm yr^{-1}] (the sum of snowfall and rainfall) (b) snowfall [mm yr^{-1}], (c) rainfall [mm yr^{-1}] and (d) mean integrated vapor transport (IVT) [$\text{kg m}^{-1} \text{s}^{-1}$] for years 480-500 over the first year ice sheet extent. The dashed black lines depict contour lines for every 500 m elevation of the 2-way simulation. The light blue line represents the ELA of the 2-way simulation. Hatches denote areas in which the differences between the 1- and 2-way coupled simulations have not become significant before the year 500.

the summer NAO index and GBI in the 1-way case ($\rho = 0.52$). However, we find no correlation in the 2-way case ($\rho = 0.00$). This shows that GrIS surface lowering can lead to a decoupling of Greenland blocking and the NAO in summer.

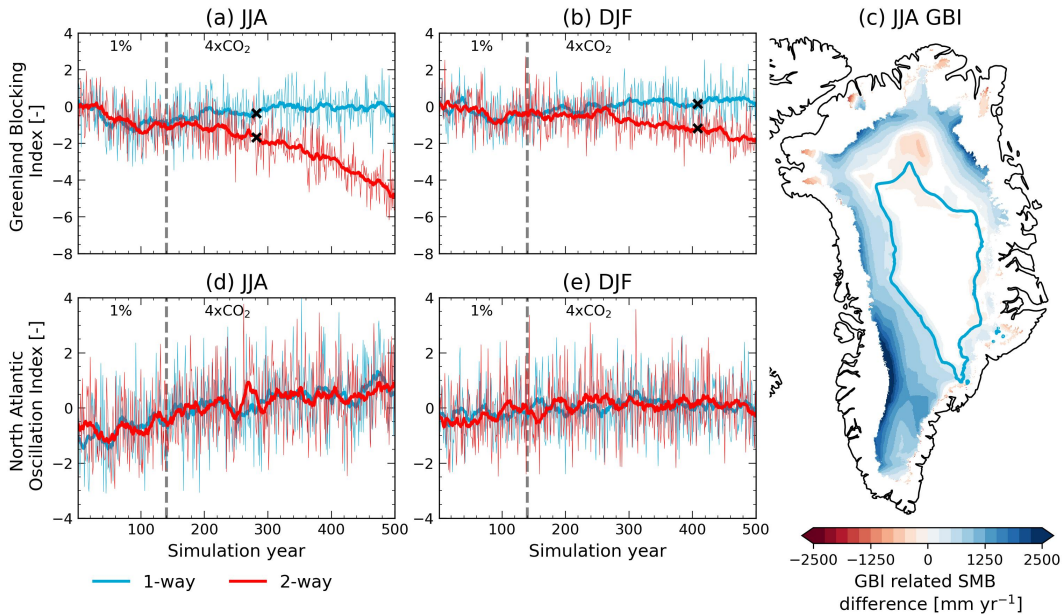


Figure 7. Evolution of (a, b) Greenland blocking index (GBI) [-] and (d, e) North Atlantic oscillation (NAO) index [-] for (a, d) June, July, August (JJA) mean and (b, e) December, January, February (DJF) mean for the 1-way (blue) and 2-way (red) coupled simulations. The grey dashed line indicates the end of the 1 % CO_2 ramp-up period and the start of the continuous $4\times\text{CO}_2$ period. If the differences between the 1- and 2-way coupled simulations become significant throughout the simulation, the first year of significant difference is marked with a black cross. (c) shows the difference in SMB [mm yr^{-1}] caused by the coupling that can be explained by the difference in summer blocking, computed using linear regression for the area with significant Pearson correlation ($p = 0.01$) for the years 480-500, for grid points that have not deglaciated in both simulations. The light blue line represents the ELA in the 2-way simulation in years 480-500.

To assess the effect of the decreased blocking on mass loss, we regress the GBI differences between the 1- and 2-way coupled simulation onto the SMB differences (from CISM2, Figure 7c). The relationship between the GBI and SMB differences is

280 strongest in the ablation area. In the accumulation zone, the surface melt is limited and therefore we do not expect a strong response to changes in Greenland blocking. As the topographies of the two simulations evolve differently, so does the SMB pattern, resulting in small areas in which the correlation signal is opposite, indicating a slightly larger SMB reduction in the 2-way coupled simulation. This might not be caused by the differences in blocking, but rather by differences in the topography. Considering areas with significantly strong correlation (as tested with a t-test using $p = 0.01$), we can link 49 % of the SMB
 285 reduction in the 2-way simulation at the end of the simulation to the decrease in atmospheric blocking (Figure 7c). As the SMB differences are mainly dominated by melt differences in this period, we hypothesize that the decrease in blocking as a result of GrIS surface elevation changes acts as a negative feedback on surface melting.

We find another negative feedback related to clouds and water vapor. Under increasing temperatures, the atmosphere can contain more moisture (as described by the Clausius-Clapeyron relationship), which can lead to an increase in clouds and enhanced precipitation (Pall et al., 2007). The amount of precipitable water in the atmospheric column (Figure 8d) increases in both simulations, although stronger in the 2-way coupled simulation, as the atmospheric column warms more and becomes thicker as a result of elevation change. The increase in precipitable water translates to a stronger reflection and absorption of incoming solar radiation in the atmosphere (Figure 8a). The differences in the atmospheric effect on incoming shortwave radiation and precipitable water both become significant in year 262, indicating they are strongly related. Although there is no
 295 increase in cloud cover (Figure 8b) in both simulations and even a slight decrease in medium-level clouds, the cloud water path (Figure 8c) increases, meaning clouds become thicker. These thicker clouds reflect more shortwave radiation, and this effect is stronger than the effect resulting from the slight decrease in cloud cover, resulting in a stronger cloud effect on incoming surface solar radiation (Figure 8a). The differences in cloud water path and cloud effect on downwelling shortwave radiation both become significant in year 401.

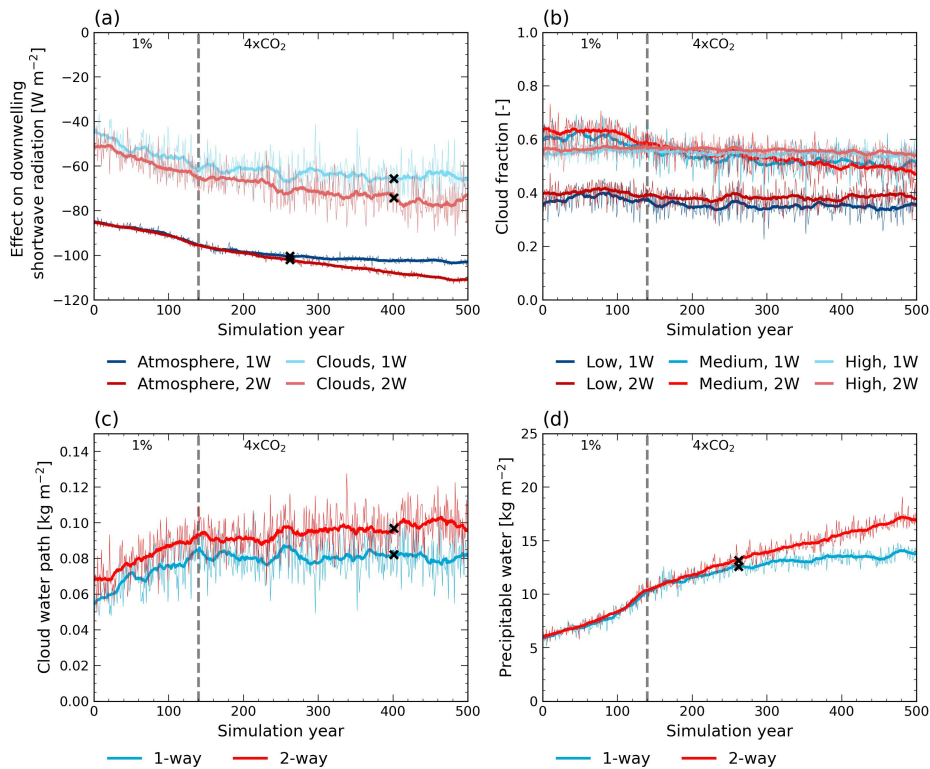


Figure 8. Timeseries of 1-way (blue, 1W) and 2-way (red, 2W) coupled simulations for (a) atmosphere and cloud effect on downwelling shortwave radiation [W m^{-2}], computed by comparing the solar insolation with the received radiation at the surface for cloud-free and cloudy conditions, (b) cloud fraction [-] for low-, medium- and high-level clouds, (c) cloud water path [kg m^{-2}] and (d) precipitable water in the atmospheric column [kg m^{-2}]. The grey dashed line indicates the end of the 1 % CO₂ ramp-up period and the start of the continuous 4xCO₂ period. If the differences between the 1- and 2-way coupled simulations become significant throughout the simulation, the first year of significant difference is marked with a black cross.

The 4xCO₂ forcing triggers large responses in global, Arctic and GrIS temperatures (Figure 9b). By year 350, the GrIS has a strongly negative mass balance (Figure 9d) causing an SLR rate of 5.7 mm yr⁻¹, with a cumulative GrIS-induced SLR of 1.13 m (Figure 9e). The discharge contribution to the mass balance is limited (-76 Gt yr⁻¹), as the ice sheet has strongly retreated. Besides, the NAMOC has collapsed (Figure 9c), reducing the amount of northward heat transport. We apply an annual 5.0 %

305 CO₂ reduction until PI CO₂ is reached (Figure 9a) to assess the GrIS mass balance and climate response to CO₂ reduction. This large CO₂ reduction can influence global, regional and local climates. We first consider global, Arctic and North Atlantic climate change and evaluate GrIS mass loss response to CO₂ reduction. We zoom in to the transition phase by looking at the NAMOC evolution and its impact on regional climate. Finally, we assess GrIS surface processes by considering the response of the snowpack.

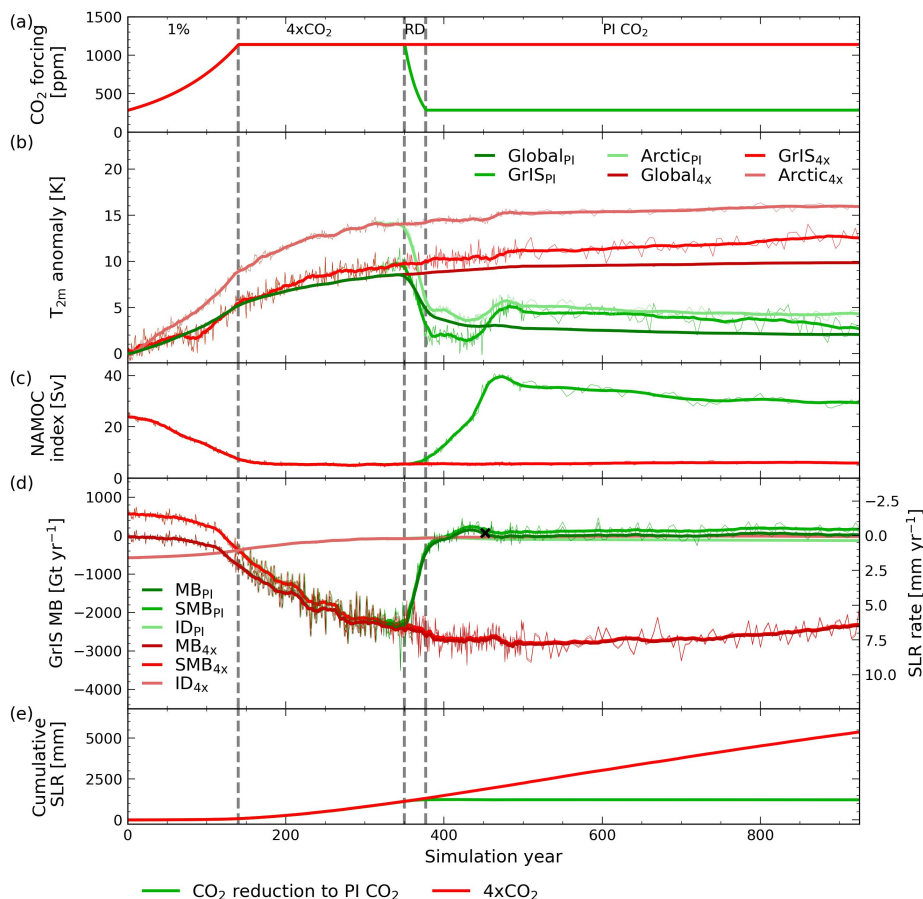


Figure 9. Evolution of CO₂ reduction to pre-industrial CO₂ (green, PI) and the full 4xCO₂ (red, 4x) simulations for (a) CO₂ forcing [ppm], (b) global, GrIS and Arctic near-surface air temperature (T_{2m}) anomalies with respect to PI [K], (c) North Atlantic Meridional Overturning Circulation (NAMOC) index [Sv], (d) GrIS total mass balance (MB) [Gt yr⁻¹] and its components ice discharge (ID) and surface mass balance (SMB) (the basal mass balance is not displayed as its contribution is limited) and (e) GrIS induced cumulative sea level rise [mm]. The mass balance (components) in (d) can be directly converted to the GrIS-induced SLR rate [mm yr⁻¹]. The grey dashed lines indicate the end of the 1% CO₂ ramp-up, the continuous 4xCO₂, the ramp-down (RD) to PI CO₂ and the continuous PI CO₂ periods. If a variable has recovered throughout the simulation, the first year of recovery is marked with a black cross.

310 The response to CO₂ reduction can be divided into two periods. During the first period, spanning the CO₂ ramp-down period and the following 85 years, the GrIS experiences a complex transitional phase because of large interactions with the NAMOC. During this phase, the NAMOC is still weak, as its recovery is delayed compared to the atmospheric response, resulting in relatively cold temperatures in the Arctic and over the GrIS (Figure 9b). Under these largely reduced air temperatures resulting from the CO₂ decrease and weak state of the NAMOC, the amount of GrIS melt decreases strongly, resulting in a small positive

315 SMB and MB (Figure 9d). During the CO₂ ramp-down and first years thereafter, there is an additional SLR of 118 cm. This

is followed by a short period (year 413 to 461) of positive mass balance, leading to a 13.4 cm sea level drop, after which GrIS-induced SLR is halted (Figure 9d, e). The second period, spanning from the end of the transitional phase to the end of the simulation, is characterized by an initial temperature increase as a response to an overshooting rebound of the NAMOC, followed by a slow continuous decrease in atmospheric temperature and NAMOC strength. The mass balance becomes smaller than during the transitional phase, nearing zero, and has recovered to its PI state by the year 452 (Table A1). However, from year 735 onward, the mass balance becomes slightly positive again, leading to an annual sea level drop of 0.06 mm yr^{-1} at the end of the simulation. This indicates that there might be potential for ice sheet regrowth, although this would likely take thousands of years. At the end of the simulation, both the SMB and ice discharge have not recovered (Table A1), but their contrasting sign allows for a near-zero mass balance, even though global and GrIS temperatures remain elevated at the end of the simulation compared to the initial state. We compare this to the state of the GrIS under the same global T_{2m} anomaly (2 K) during the CO_2 ramp-up (year 70), where we see an ice sheet that is largely marine-terminating and is out of balance as a result of this temperature anomaly (Table 2). Although the ice sheet has a stronger positive SMB in year 70, the large ice discharge leads to net mass loss, while for the retreated ice sheet at the end of the CO_2 reduction simulation, the total mass balance is slightly positive, despite the smaller SMB.

Table 2. Comparison of the state of the GrIS under an annual global T_{2m} anomaly of 2.0 K during the CO_2 ramp-up period in year 70 (average over years 60-80) and at the end of the CO_2 reduction simulation (average over years 825-925). The number within brackets represents one standard deviation.

	Year 70 (60-80 mean)	End of simulation (825-925 mean)
Global T_{2m} anomaly	2.0 (0.22) K	2.0 (0.08) K
GrIS T_{2m} anomaly	1.9 (0.68) K	2.9 (1.0) K
Total mass balance	-105 (76) Gt yr^{-1}	21 (70) Gt yr^{-1}
SMB	438 (81) Gt yr^{-1}	161 (70) Gt yr^{-1}
Integrated SMB	224 (40) mm yr^{-1}	103 (43) mm yr^{-1}
Ice discharge	-520 (7.0) Gt yr^{-1}	-124 (4.8) Gt yr^{-1}

During the $4x\text{CO}_2$ forcing period, the North Atlantic warms less rapidly due to the weakening of the NAMOC, resulting in a warming hole southeast of Greenland (Figure 10a). During the transitional CO_2 reduction phase, the North Atlantic cools rapidly as this warming hole persists under a weak NAMOC (Figure 10c). However, the delayed NAMOC overshoot causes the North Atlantic temperatures to rise subsequently, causing a cooling hole in the area south of Greenland (Figure 10e). Besides, the timing of changes in GrIS, North Atlantic and Arctic processes strongly coincides with the timing of NAMOC index changes (Figure A6), highlighting the complexity of the interactions between the ocean, atmosphere, Arctic sea ice and the GrIS.

The Arctic interacts strongly with the NAMOC and the atmosphere. Due to a large drop in Arctic T_{2m} as a response to reverting CO_2 conditions, the March Arctic sea ice extent recovers quickly (Figure 10b), amplified by the thin ice feedback (Notz, 2009) and the sea ice-albedo feedback (Curry et al., 1995). In contrast, the September sea ice does not recover, since the newly formed sea ice is relatively thin (Figure 10d) and ocean and atmosphere summer temperatures remain elevated, leading to the nearly complete melting of the recently formed sea ice in summer. The regrowth of sea ice influences the NAMOC strength, as brine rejection leads to more saline high-latitude waters, enhancing overturning. The overshooting response of the NAMOC leads to a subsequent decrease in Arctic sea ice extent and thickness as a result of increased northward heat transport.

The mixed layer depth (MLD, Figure 10f), which is an indicator for the amount of overturning and thus for the strength of the NAMOC, decreases in the Labrador Sea, Irminger Sea and the Norwegian Sea when CO_2 concentrations are increased. In contrast, the MLD in the Nansen Basin starts to increase slightly. This indicates a movement of the area with strong overturning towards higher latitudes, possibly caused by the decrease in Arctic sea ice extent (Figure 10b). The MLDs in the Labrador Sea, Irminger Sea and Norwegian Sea all experience an overshoot after the CO_2 ramp-down, similar to the NAMOC index. Only

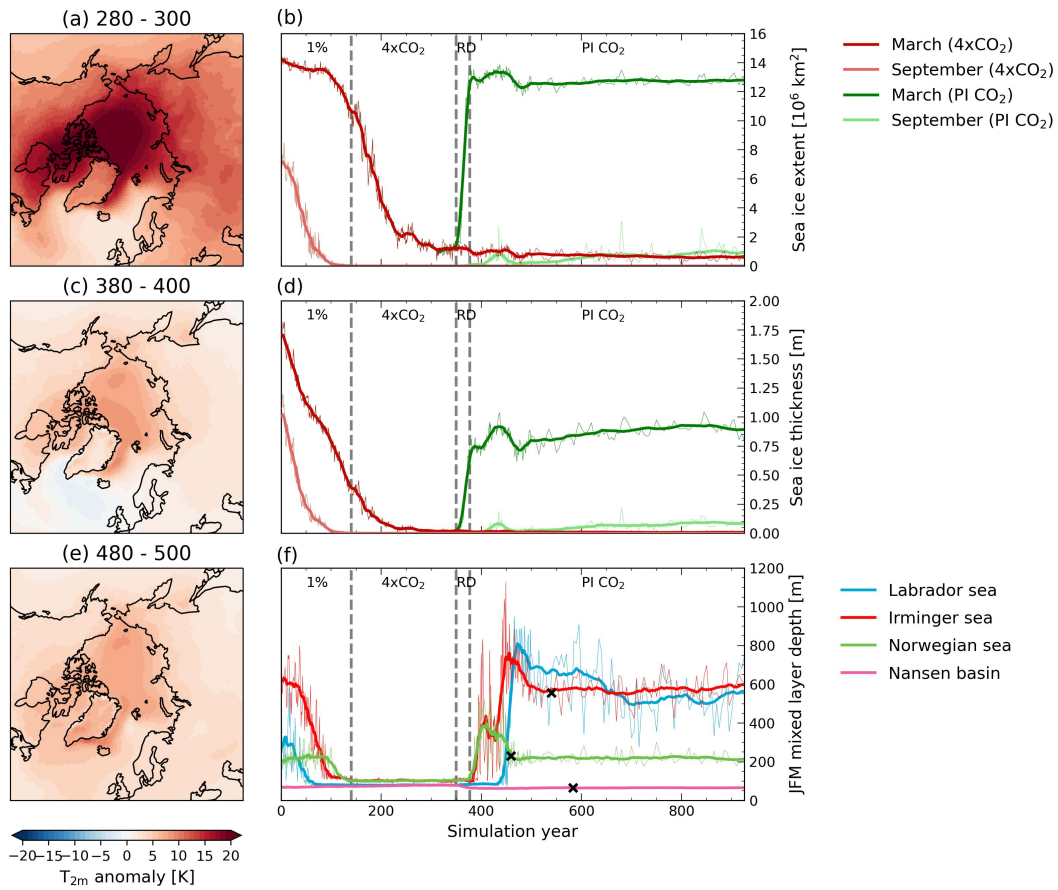


Figure 10. (a, c, e) Evolution of the anomalies of the global near-surface temperature (T_{2m}) [K] for the CO₂ reduction simulation compared to the control simulation for (a) years 280-300 during the constant 4xCO₂ period, (c) years 380-400 just after the CO₂ ramp-down in the transition period and (e) years 480-500 after the transition period. (b, d) Evolution of reduction to pre-industrial CO₂ (green) and the full 4xCO₂ (red) simulations for (b) sea ice extent [10^6 km^2] and (d) sea ice thickness [m] in March and September. (f) Evolution of the mean mixed layer depth (MLD) of January, February and March (JFM) in the Labrador Sea (blue), Irminger Sea (red), Norwegian Sea (green) and Nansen Basin (pink) for the reduction to pre-industrial CO₂ simulation. In (b, d, f) the grey dashed lines indicate the end of the 1 % CO₂ ramp-up, the continuous 4xCO₂, the ramp-down (RD) to PI CO₂ and the continuous PI CO₂ periods. If a variable has recovered throughout the simulation, the first year of recovery is marked with a black cross.

in the Labrador Sea, there is no complete recovery from the overshoot, which is where we see the large remaining temperature anomalies as well (Figure 10c), indicating elevated heat transport.

Looking at GrIS surface processes, we find that melt increases due to the CO₂ forcing, are partly countered by enhanced refreezing (Figure 11a). At the end of the ramp-up period, in the year 130, the peak in refreezing is reached, despite the ongoing increase in the amount of available water for refreezing. This implies that around this year the pore space and/or available energy for melt has started to decrease. This peak refreezing behavior is typical for high emission scenarios (Noël et al., 2022). After the CO₂ ramp-down, the refreezing slightly peaks again in year 478, as the snowpack partially recovers. However, the poorer state of the snow compared to its state before the 4xCO₂ forcing was applied, characterized by higher snow temperatures and a thinner snowpack (Figure A7), prevents the snowpack from returning to refreezing rates similar to year 130, despite the similar amount of available water, resulting in a refreezing capacity that does not recover (Table A1).

Next to the refreezing, the ice sheet albedo does not completely recover either (Figure 11b). In the cooler period around years 400 to 450, the albedo nearly recovers to its initial state, even around the margins, as melt strongly reduces. However, subsequent temperature increases due to the NAMOC recovery lead to more melt and rain and a corresponding decrease in albedo, aligning with the expansion of the ablation area, resulting in an ELA that does not recover. The lower surface albedo causes the net shortwave flux to remain larger, which is the largest contributor to the fact that the SMB and SEB (Figure A5) do not recover completely.

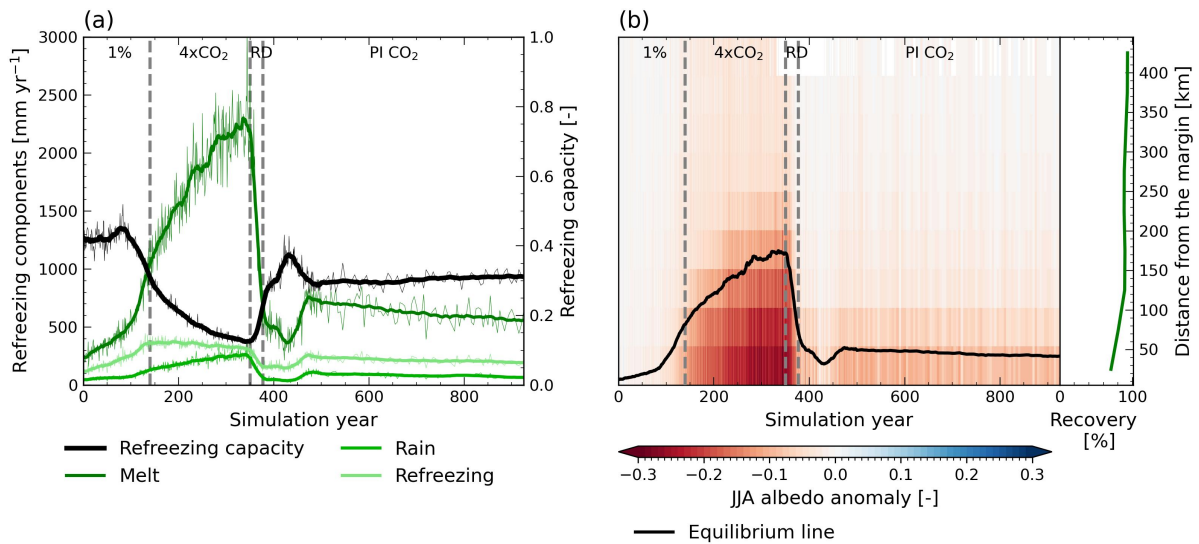


Figure 11. Evolution of the snow properties (a) refreezing capacity (black) [-] and its components meltwater (dark green), rainfall (green) and refreezing (light green) [mm yr⁻¹] and (b) summer (JJA) albedo anomalies [-] with respect to the control simulation as a function of time and distance to the ice sheet margin for the reintroduction of PI CO₂ simulation and the location of the equilibrium line (black). In (b), the dark green line shows the relative recovery (in %) for each distance class. The grey dashed lines indicate the end of the 1 % CO₂ ramp-up, the continuous 4xCO₂, the ramp-down (RD) to PI CO₂ and the continuous PI CO₂ periods. None of the variables in (a) have recovered by the end of the simulation.

365 6 Discussion

The results presented in this study highlight the importance of accounting for interactions between the GrIS and the climate for SLR projections. We find that parameterizing ice sheet-climate interactions leads to a consistent overestimation of the GrIS-induced SLR of 17 % under a 4xPI CO₂ forcing throughout the simulation. Similarly, Ridley et al. (2005) found an overestimation of mass loss in an uncoupled AOGCM-ISM simulation, although these only become apparent after a total mass
 370 loss of around 2.5 m SLE, opposed to 0.7 m SLE in our study. Our results are close to those of Gregory et al. (2020), who found a relative overestimation of mass loss of 13 % in an uncoupled abrupt 4xCO₂ simulation using the Glimmer ice sheet model coupled to FAMOUS-ice. Gregory et al. (2020) attributed part of the smaller mass loss in the coupled simulation to a larger precipitation increase, as precipitation in the southwest moves land inward, which is similar to what we find. However, the larger rainfall does not contribute positively to the SMB and although the snowfall in the accumulation area is larger in
 375 the 2-way coupled simulation, its contribution is limited (28 Gt yr⁻¹ by year 500, Figure A4). Besides, Gregory et al. (2020) related the smaller mass to a negative cloud feedback on the downwelling shortwave radiation due to a larger cloud fraction in the coupled simulation. Although we do not find significant differences in cloud fraction, we find significantly thicker clouds in the 2-way coupled simulation, resulting in a similar cloud feedback on solar radiation. It may be noted that we find an initial difference between the two simulations in cloud-related variables, which, however non-significant in year 1, can influence our
 380 results. Whether these differences are related to internal variability or are related to the model set-up is being investigated.

Contrasting to Ridley et al. (2005) and Gregory et al. (2020), we find a large influence of atmospheric blocking on SMB evolution. In our 2-way coupled simulation, blocking is significantly reduced and is linked with nearly half of the difference in SMB reduction, acting as negative feedback on surface melt. Observations and climate projections show that blocking has a strong effect on GrIS melting (Sellevold and Vizcaíno, 2020; Hanna et al., 2022). However, Hanna et al. (2018) showed that
 385 climate models are not able to capture the present-day increase in GBI and consistently project a future decrease in blocking. Therefore blocking projections should be treated with caution. Nevertheless, the significant decrease in GBI in our 2-way simulation is related to large topographic changes, which are not the main driver of present-day GBI changes.

Besides, we hypothesize that a large part of the larger mass loss in the 1-way simulation arises from the application of a uniform T_{2m} lapse rate. Compared to the lapse rates computed from our 1- and 2-way simulations, the applied uniform lapse

390 rate results in an overestimation of summer T_{2m} in the ablation area and therefore melt might be overestimated. Although the use of uniform lapse rates in offline simulations is common (e.g. Aschwanden et al., 2019; Sellevold and Vizcaíno, 2020; Bochow et al., 2023), it has been pointed out that lapse rates are not temporally and spatially uniform (Hanna et al., 2005; Gardner et al., 2009) and that the melt-elevation feedback is sensitive to the choice of the lapse rate (Zeitz et al., 2022). Crow et al. (2023, preprint) found that applying a seasonally and spatially varying lapse rate for downscaling SMB from 1-way
395 coupled CESM simulations of the MIS-11c Greenland Ice Sheet gives the most accurate representation of the melt-elevation feedback, showing that it is likely that offline corrections in ice sheet models can be improved by accounting for the temporal variability of the lapse rate in the ablation area. It should be noted that our computed T_{2m} lapse rates are not only affected by the surface reaching melting point but also by the other negative feedbacks influencing temperature, like increasing cloud thickness and reduced atmospheric blocking.

400 When we apply a 5 % CO_2 reduction to PI CO_2 , we find that GrIS-induced SLR can be halted. However, the chosen CO_2 forcing, the timing and the rate of the CO_2 ramp-up and ramp-down likely have a large influence on the mass balance evolution and influence whether mass loss can be halted or reversed. In our simulation, a small positive mass balance, during the transitional phase just after CO_2 reduction, as well as at the end of the simulation, allows for a small regrowth of the ice sheet. However, reversing the 1.1 m (equal to 14 % of the initial ice sheet volume) of mass lost during the forcing period would
405 likely take thousands of years. Our simulation is designed to investigate the response of the GrIS to CO_2 reduction and the climate interactions that play a role therein, rather than finding thresholds for irreversible mass loss and potential equilibrium states, in contrast to previous work. Despite the long time scales used in previous work, the importance of certain feedbacks and interactions has been pointed out before. Using a coupled AOGCM-ISM configuration, Ridley et al. (2010) investigated the potential regrowth of the GrIS from 11 different initial states when reverting to PI climate. They showed that for states with an
410 ice sheet area reduction of 10 % and 20 %, which is in the same order as this study, climate-ice sheet interactions, resulting from the temperature dependence on elevation, make the difference in whether or not the ice sheet could regrow. Although in the study by Ridley et al. (2010) the ice sheet is coupled to the ocean model, interactions with the NAMOC are likely not captured due to the experimental set-up with asynchronous coupling. Using the FAMOUS-ice - GLIMMER coupled configuration, Gregory et al. (2020) performed CO_2 removal experiments starting from multiple GrIS (steady) states and highlighted the
415 importance of the melt-albedo feedback on reversibility, which our results agree with. Their mass loss trajectories do not show a complex transitional phase as the model set-up does not allow for interaction with the ocean, meaning there is no influence from an overshooting NAMOC recovery. Bochow et al. (2023) used two ice sheet models to explore the GrIS mass balance response to a linear temperature ramp-up and subsequent ramp-down. Their experiment with a 100 year ramp-up to 7 K warming followed by a 100 year ramp-down to a remaining 2 K warming and an additional simulated 100 kyr at this 2 K
420 warming level, is closest to our experiment. Depending on the model, they find a notable larger mass loss of 2 to 6 m SLE, although over a larger time scale. However, at the end of our simulation, the ice sheet has a small, but positive mass balance, and therefore we do not expect the ice sheet to lose more mass if we would extend the simulation. The study by Bochow et al. (2023) only includes limited interactions between the ice sheet and the atmosphere (melt-elevation and melt-albedo feedback and precipitation changes) and no interactions with the ocean. These differences show the large impact of complex climate-ice
425 sheet interactions on projected mass loss.

The large impact of interactions with the NAMOC in the transitional phase towards a colder climate is apparent in this study and is not discussed in other studies on GrIS mass loss behavior in CO_2 reduction scenarios. However, the response of the (N)AMOC to CO_2 reduction has been studied under similar 1 % ramp-up and ramp-down $4\times CO_2$ scenarios (Wu et al., 2011; An et al., 2021; Oh et al., 2022). There is agreement on the existence of overshoot behavior of the AMOC, reaching AMOC
430 strengths larger than in the PI climate, and this response is delayed compared to the atmospheric response to CO_2 reduction. This behavior is mainly attributed to the enhanced salt-advection feedback. Our study only focuses on interactions with the Arctic and North Atlantic. Hence, changes in salinity in the subtropics resulting from an intensification of the hydrological cycle (Wu et al., 2011) are not taken into consideration in our analysis. Therefore, our assessment of NAMOC changes related

to changes in the Arctic and North Atlantic describes interactions between and dependencies on the different processes in these
435 areas, rather than attributing causes and effects of NAMOC changes.

7 Conclusions

In this study, we made an extensive comparison of the 1- and 2-way coupled configuration of CESM2-CISM2, to investigate topography-related feedback mechanisms and assess how well 1-way coupling can capture the elevation feedbacks. We find that in a 4xCO₂ scenario, the sum of topography-related feedback responses results in 66 % more melt by year 500 when
440 considering a dynamic GrIS by using 2-way coupling. However, the offline topography correction in CISM2 in the 1-way configuration overestimates these feedbacks, resulting in an overestimation of mass loss of 17 % in the 1-way simulation. This overestimation partly arises from the overestimation of the positive melt-elevation and melt-albedo feedbacks, as well as not including several negative atmospheric feedback mechanisms. In the 1-way coupled simulation, a uniform temperature lapse rate of -6 K is used to correct for elevation changes. However, the temperature lapse has a large seasonal variability,
445 as the surface in the ablation area is at melting point in summer. Overestimated temperature lapse rates in summer result in an overestimation of the melt-elevation feedback, which enhances the melt-albedo feedback as well. Taking this seasonal dependency into account when doing offline corrections for elevation could help resolve part of the discrepancy between the 1- and 2-way coupled simulations. Besides, the changes in GrIS topography result in increased precipitation, reduced atmospheric blocking and a decrease in solar radiation reaching the surface resulting from increased atmospheric water vapor content and
450 cloud thickness. These atmospheric responses act as negative feedbacks on melt, resulting in smaller mass loss in the 2-way coupled simulation. These results stress the importance of considering ice sheet-climate interactions for SLR projections, by using 2-way coupled simulations.

A rapid reduction of atmospheric CO₂ from 4xPI to 1xPI conditions leads to strong responses of the global, GrIS and Arctic climate. Despite a remaining global temperature anomaly of 2 K, compared to the initial PI climate, GrIS mass loss halts,
455 resulting from the small contribution of discharge as the ice sheet has partially retreated under a total mass loss of 1.1 m SLE. The collapsed NAMOC results in a warming hole south of Greenland during the forcing period and the first years after the CO₂ ramp-down, but eventually recovers and overshoots under the reintroduced PI CO₂, resulting in a cooling hole in this area. This results in a complex transitional phase in which temperatures first decrease rapidly but increase subsequently. Arctic sea ice extent in winter recovers well, but the ice remains thin and largely melts away in summer. As a result, Arctic temperatures
460 remain high. Although the GrIS mass balance recovers, its SMB does not, resulting from elevated temperatures, elevated ocean heat transport, and a snowpack that does not recover compared to the initial PI state. The refreezing capacity of the snowpack reduces as a result of a smaller snow depth and higher snow temperatures. Besides, the albedo of the snowpack remains lower, leading to a stronger melt-albedo feedback.

This idealized CO₂ ramp-down scenario shows the importance of ice sheet-climate interactions on the response of the GrIS
465 mass balance and climate to CO₂ reduction. Overshoot scenarios are becoming more important in policy-making, while studies regarding GrIS mass loss reversibility focus on multi-millennial behavior and do not always account for interactions with the climate (e.g. in: Ridley et al., 2005; Gregory et al., 2020; Bochow et al., 2023). Although this study is a first step towards understanding GrIS mass balance evolution under CO₂ reduction, considering shorter-term simulations and less rapid ramp-down scenarios is crucial for SLR projections. In short-term simulations, SLR might not be halted when decreasing CO₂
470 concentrations, as discharge contributes more to the mass balance, and the interactions with the NAMOC could be smaller, as the magnitude of the NAMOC response to CO₂ reduction depends on how large the CO₂ forcing is and for how long it is applied (Wu et al., 2011).

References

- An, S.-I., Shin, J., Yeh, S.-W., Son, S.-W., Kug, J.-S., Min, S.-K., and Kim, H.-J.: Global Cooling Hiatus Driven by an AMOC Overshoot in a Carbon Dioxide Removal Scenario, *Earth's Future*, 9, e2021EF002165, <https://doi.org/10.1029/2021EF002165>, 2021.
- Aschwanden, A., Fahnestock, M. A., Truffer, M., Brinkerhoff, D. J., Hock, R., Khroulev, C., Mottram, R., and Khan, S. A.: Contribution of the Greenland Ice Sheet to sea level over the next millennium, *Science Advances*, 5, <https://doi.org/10.1126/sciadv.aav9396>, 2019.
- Bamber, J. L., Oppenheimer, M., Kopp, R. E., Aspinall, W. P., and Cooke, R. M.: Ice sheet contributions to future sea-level rise from structured expert judgment, *Proceedings of the National Academy of Sciences*, 116, 11 195–11 200, <https://doi.org/10.1073/pnas.1817205116>, 2019.
- 475 Blanke, B., Arhan, M., and Speich, S.: Salinity changes along the upper limb of the Atlantic thermohaline circulation, *Geophysical Research Letters*, 33, <https://doi.org/10.1029/2005GL024938>, 2006.
- Bochow, N., Poltronieri, A., Robinson, A., Montoya, M., Rypdal, M., and Boers, N.: Overshooting the critical threshold for the Greenland ice sheet, *Nature*, 622, 528–536, <https://doi.org/10.1038/s41586-023-06503-9>, 2023.
- Box, J. E., Fettweis, X., Stroeve, J. C., Tedesco, M., Hall, D. K., and Steffen, K.: Greenland ice sheet albedo feedback: thermodynamics and atmospheric drivers, *The Cryosphere*, 6, 821–839, <https://doi.org/10.5194/tc-6-821-2012>, 2012.
- 485 Bretones, A., Nisancioglu, K. H., Jensen, M. F., Brakstad, A., and Yang, S.: Transient Increase in Arctic Deep-Water Formation and Ocean Circulation under Sea Ice Retreat, *Journal of Climate*, 35, 109–124, <https://doi.org/10.1175/JCLI-D-21-0152.1>, 2022.
- Crow, B. R., Tarasov, L., Schulz, M., and Prange, M.: Uncertainties originating from GCM downscaling and bias correction with application to the MIS-11c Greenland Ice Sheet, *EGUsphere* [preprint], 2023, <https://doi.org/10.5194/egusphere-2023-1367>, 2023.
- 490 Curry, J. A., Schramm, J. L., and Ebert, E. E.: Sea Ice-Albedo Climate Feedback Mechanism, *Journal of Climate*, 8, 240–247, [https://doi.org/10.1175/1520-0442\(1995\)008<0240:SIACFM>2.0.CO;2](https://doi.org/10.1175/1520-0442(1995)008<0240:SIACFM>2.0.CO;2), 1995.
- Danabasoglu, G., Lamarque, J.-F., Bacmeister, J., Bailey, D. A., DuVivier, A. K., Edwards, J., Emmons, L. K., Fasullo, J., Garcia, R., Gettelman, A., Hannay, C., Holland, M. M., Large, W. G., Lauritzen, P. H., Lawrence, D. M., Lenaerts, J. T. M., Lindsay, K., Lipscomb, W. H., Mills, M. J., Neale, R., Oleson, K. W., Otto-Bliesner, B., Phillips, A. S., Sacks, W., Tilmes, S., van Kampenhout, L., Vertenstein, M., Bertini, A., Dennis, J., Deser, C., Fischer, C., Fox-Kemper, B., Kay, J. E., Kinnison, D., Kushner, P. J., Larson, V. E., Long, M. C., Mickelson, S., Moore, J. K., Nienhouse, E., Polvani, L., Rasch, P. J., and Strand, W. G.: The Community Earth System Model Version 2 (CESM2), *Journal of Advances in Modeling Earth Systems*, 12, <https://doi.org/10.1029/2019MS001916>, e2019MS001916, 2020.
- 495 Dangendorf, S., Hay, C., Calafat, F. M., Marcos, M., Piecuch, C. G., Berk, K., and Jensen, J.: Persistent acceleration in global sea-level rise since the 1960s, *Nature Climate Change*, 9, 705–710, <https://doi.org/10.1038/s41558-019-0531-8>, 2019.
- 500 Davini, P., Cagnazzo, C., Neale, R., and Tribbia, J.: Coupling between Greenland blocking and the North Atlantic Oscillation pattern, *Geophysical Research Letters*, 39, <https://doi.org/10.1029/2012GL052315>, 2012.
- Driesschaert, E., Fichet, T., Goosse, H., Huybrechts, P., Janssens, I., Mouchet, A., Munhoven, G., Brovkin, V., and Weber, S. L.: Modeling the influence of Greenland ice sheet melting on the Atlantic meridional overturning circulation during the next millennia, *Geophysical Research Letters*, 34, <https://doi.org/10.1029/2007GL029516>, 2007.
- 505 Edwards, T. L., Fettweis, X., Gagliardini, O., Gillet-Chaulet, F., Goelzer, H., Gregory, J. M., Hoffman, M., Huybrechts, P., Payne, A. J., Perego, M., Price, S., Quiquet, A., and Ritz, C.: Effect of uncertainty in surface mass balance–elevation feedback on projections of the future sea level contribution of the Greenland ice sheet, *The Cryosphere*, 8, 195–208, <https://doi.org/10.5194/tc-8-195-2014>, 2014.
- Flanner, M. G., Arnheim, J. B., Cook, J. M., Dang, C., He, C., Huang, X., Singh, D., Skiles, S. M., Whicker, C. A., and Zender, C. S.: SNICAR-ADv3: a community tool for modeling spectral snow albedo, *Geoscientific Model Development*, 14, 7673–7704, <https://doi.org/10.5194/gmd-14-7673-2021>, 2021.
- 510 Fox-Kemper, B., Hewitt, H., Xiao, C., Aðalgeirsdóttir, G., Drijfhout, S., Edwards, T., Golledge, N., Hemer, M., Kopp, R., Krinner, G., Mix, A., Notz, D., Nowicki, S., Nurhati, I., Ruiz, L., Sallée, J.-B., Slangen, A., and Yu, Y.: Ocean, Cryosphere and Sea Level Change. In *Climate Change 2021: The Physical Science Basis. Contribution of Working Group I to the Sixth Assessment Report of the Intergovernmental Panel on Climate Change* [Masson-Delmotte, V., P. Zhai, A. Pirani, S.L. Connors, C. Péan, S. Berger, N. Caud, Y. Chen, L. Goldfarb, M.I. Gomis, M. Huang, K. Leitzell, E. Lonnoy, J.B.R. Matthews, T.K. Maycock, T. Waterfield, O. Yelekçi, R. Yu, and B. Zhou (eds.)], Cambridge University Press, Cambridge, United Kingdom and New York, NY, USA, pp. 1211–1362, <https://doi.org/10.1017/9781009157896.011>, 2021.
- 515 Fyke, J., Sergienko, O., Löfverström, M., Price, S., and Lenaerts, J. T. M.: An Overview of Interactions and Feedbacks Between Ice Sheets and the Earth System, *Reviews of Geophysics*, 56, 361–408, <https://doi.org/10.1029/2018RG000600>, 2018.
- 520 Fyke, J. G., Vizcaíno, M., and Lipscomb, W. H.: The pattern of anthropogenic signal emergence in Greenland Ice Sheet surface mass balance, *Geophysical Research Letters*, 41, 6002–6008, <https://doi.org/10.1002/2014GL060735>, 2014.

- Fürst, J. J., Goelzer, H., and Huybrechts, P.: Ice-dynamic projections of the Greenland ice sheet in response to atmospheric and oceanic warming, *The Cryosphere*, 9, 1039–1062, <https://doi.org/10.5194/tc-9-1039-2015>, 2015.
- 525 Gardner, A. S., Sharp, M. J., Koerner, R. M., Labine, C., Boon, S., Marshall, S. J., Burgess, D. O., and Lewis, D.: Near-Surface Temperature Lapse Rates over Arctic Glaciers and Their Implications for Temperature Downscaling, *Journal of Climate*, 22, 4281–4298, <https://doi.org/10.1175/2009JCLI2845.1>, 2009.
- Gettelman, A., Mills, M. J., Kinnison, D. E., Garcia, R. R., Smith, A. K., Marsh, D. R., Tilmes, S., Vitt, F., Bardeen, C. G., McInerney, J., Liu, H.-L., Solomon, S. C., Polvani, L. M., Emmons, L. K., Lamarque, J.-F., Richter, J. H., Glanville, A. S., Bacmeister, J. T., Phillips, A. S., Neale, R. B., Simpson, I. R., DuVivier, A. K., Hodzic, A., and Randel, W. J.: The Whole Atmosphere Community Climate Model Version 6 (WACCM6), *Journal of Geophysical Research: Atmospheres*, 124, 12 380–12 403, <https://doi.org/10.1029/2019JD030943>, 2019.
- 530 Goelzer, H., Huybrechts, P., Fürst, J. J., Nick, F. M., Andersen, M. L., Edwards, T. L., Fettweis, X., Payne, A. J., and Shannon, S.: Sensitivity of Greenland Ice Sheet Projections to Model Formulations, *Journal of Glaciology*, 59, 733–749, <https://doi.org/10.3189/2013JoG12J182>, 2013.
- Goelzer, H., Nowicki, S., Payne, A., Larour, E., Seroussi, H., Lipscomb, W. H., Gregory, J., Abe-Ouchi, A., Shepherd, A., Simon, E., Agosta, C., Alexander, P., Aschwanden, A., Barthel, A., Calov, R., Chambers, C., Choi, Y., Cuzzone, J., Dumas, C., Edwards, T., Felikson, D., Fettweis, X., Gолledge, N. R., Greve, R., Humbert, A., Huybrechts, P., Le clec'h, S., Lee, V., Leguy, G., Little, C., Lowry, D. P., Morlighem, M., Nias, I., Quiquet, A., Rückamp, M., Schlegel, N.-J., Slater, D. A., Smith, R. S., Straneo, F., Tarasov, L., van de Wal, R., and van den Broeke, M.: The future sea-level contribution of the Greenland ice sheet: a multi-model ensemble study of ISMIP6, *The Cryosphere*, 14, 3071–3096, <https://doi.org/10.5194/tc-14-3071-2020>, 2020.
- 535 Gregory, J. M., George, S. E., and Smith, R. S.: Large and irreversible future decline of the Greenland ice sheet, *The Cryosphere*, 14, 4299–4322, <https://doi.org/10.5194/tc-14-4299-2020>, 2020.
- Gulev, S., Thorne, P.W., Ahn, J., Dentener, F.J., Domingues, C.M., Gerland, S., Gong, D., Kaufman, D.S., Nnamchi, H.C., Quaas, J., Rivera, J.A., Sathyendranath, S., Smith, S.L., Trewin, B., von Schuckmann, K., and Vose, R.S.: Changing State of the Climate System. In: *Climate Change 2021 – The Physical Science Basis: Working Group I Contribution to the Sixth Assessment Report of the Intergovernmental Panel on Climate Change* [Masson-Delmotte, V., P. Zhai, A. Pirani, S.L. Connors, C. Péan, S. Berger, N. Caud, Y. Chen, L. Goldfarb, M.I. Gomis, M. Huang, K. Leitzell, E. Lonnoy, J.B.R. Matthews, T.K. Maycock, T. Waterfield, O. Yelekçi, R. Yu, and B. Zhou (eds.)], Cambridge University Press, 1 edn., <https://doi.org/10.1017/9781009157896>, 2023.
- 545 Hanna, E., Huybrechts, P., Janssens, I., Cappelen, J., Steffen, K., and Stephens, A.: Runoff and mass balance of the Greenland ice sheet: 1958–2003, *Journal of Geophysical Research: Atmospheres*, 110, <https://doi.org/10.1029/2004JD005641>, 2005.
- 550 Hanna, E., Huybrechts, P., Steffen, K., Cappelen, J., Huff, R., Shuman, C., Irvine-Fynn, T., Wise, S., and Griffiths, M.: Increased Runoff from Melt from the Greenland Ice Sheet: A Response to Global Warming, *Journal of Climate*, 21, 331–341, <https://doi.org/10.1175/2007JCLI1964.1>, 2008.
- Hanna, E., Fettweis, X., and Hall, R. J.: Brief communication: Recent changes in summer Greenland blocking captured by none of the CMIP5 models, *The Cryosphere*, 12, 3287–3292, <https://doi.org/10.5194/tc-12-3287-2018>, 2018.
- 555 Hanna, E., Cropper, T. E., Hall, R. J., Cornes, R. C., and Barriendos, M.: Extended North Atlantic Oscillation and Greenland Blocking Indices 1800–2020 from New Meteorological Reanalysis, *Atmosphere*, 13, 436, <https://doi.org/10.3390/atmos13030436>, 2022.
- Hunke, E., Lipscomb, W., Jones, P., Turner, A., Jeffery, N., and Elliott, S.: CICE, The Los Alamos Sea Ice Model, Tech. Rep. CICE; 005315WKSTN00, Los Alamos National Laboratory (LANL), Los Alamos, NM (United States), <https://www.osti.gov/biblio/1364126>, 2017.
- 560 Hurrell, J. W.: Decadal Trends in the North Atlantic Oscillation: Regional Temperatures and Precipitation, *Science*, 269, 676–679, <https://doi.org/10.1126/science.269.5224.676>, 1995.
- Jones, G. S., Stott, P. A., and Christidis, N.: Attribution of observed historical near-surface temperature variations to anthropogenic and natural causes using CMIP5 simulations, *Journal of Geophysical Research: Atmospheres*, 118, 4001–4024, <https://doi.org/10.1002/jgrd.50239>, 2013.
- 565 Kostov, Y., Johnson, H. L., and Marshall, D. P.: AMOC sensitivity to surface buoyancy fluxes: the role of air-sea feedback mechanisms, *Climate Dynamics*, 53, 4521–4537, <https://doi.org/10.1007/s00382-019-04802-4>, 2019.
- Lawrence, D. M., Fisher, R. A., Koven, C. D., Oleson, K. W., Swenson, S. C., Bonan, G., Collier, N., Ghimire, B., van Kampenhout, L., Kennedy, D., Kluzek, E., Lawrence, P. J., Li, F., Li, H., Lombardozzi, D., Riley, W. J., Sacks, W. J., Shi, M., Vertenstein, M., Wieder, W. R., Xu, C., Ali, A. A., Badger, A. M., Bisht, G., van den Broeke, M., Brunke, M. A., Burns, S. P., Buzan, J., Clark, M., Craig, A., Dahlin, K., Drewniak, B., Fisher, J. B., Flanner, M., Fox, A. M., Gentine, P., Hoffman, F., Keppel-Aleks, G., Knox, R., Kumar, S., Lenaerts,
- 570

- J., Leung, L. R., Lipscomb, W. H., Lu, Y., Pandey, A., Pelletier, J. D., Perket, J., Randerson, J. T., Ricciuto, D. M., Sanderson, B. M., Slater, A., Subin, Z. M., Tang, J., Thomas, R. Q., Val Martin, M., and Zeng, X.: The Community Land Model Version 5: Description of New Features, Benchmarking, and Impact of Forcing Uncertainty, *Journal of Advances in Modeling Earth Systems*, 11, 4245–4287, <https://doi.org/10.1029/2018MS001583>, 2019.
- 575 Li, H., Wigmosta, M. S., Wu, H., Huang, M., Ke, Y., Coleman, A. M., and Leung, L. R.: A Physically Based Runoff Routing Model for Land Surface and Earth System Models, *Journal of Hydrometeorology*, 14, 808–828, <https://doi.org/10.1175/JHM-D-12-015.1>, 2013.
- Lipscomb, W. H., Price, S. F., Hoffman, M. J., Leguy, G. R., Bennett, A. R., Bradley, S. L., Evans, K. J., Fyke, J. G., Kennedy, J. H., Perego, M., Ranken, D. M., Sacks, W. J., Salinger, A. G., Vargo, L. J., and Worley, P. H.: Description and evaluation of the Community Ice Sheet Model (CISM) v2.1, *Geoscientific Model Development*, 12, 387–424, <https://doi.org/10.5194/gmd-12-387-2019>, 2019.
- 580 Liu, J., Chen, Z., Francis, J., Song, M., Mote, T., and Hu, Y.: Has Arctic Sea Ice Loss Contributed to Increased Surface Melting of the Greenland Ice Sheet?, *Journal of Climate*, 29, 3373–3386, <https://doi.org/10.1175/JCLI-D-15-0391.1>, 2016.
- Marshall, J. and Plumb, R. A.: Atmosphere, ocean, and climate dynamics: an introductory text, no. 93 in International geophysics series, Elsevier, 2008.
- Matthews, H. D. and Wynes, S.: Current global efforts are insufficient to limit warming to 1.5°C, *Science*, 376, 1404–1409, <https://doi.org/10.1126/science.abo3378>, 2022.
- 585 Morlighem, M., Williams, C. N., Rignot, E., An, L., Arndt, J. E., Bamber, J. L., Catania, G., Chauché, N., Dowdeswell, J. A., Dorschel, B., Fenty, I., Hogan, K., Howat, I., Hubbard, A., Jakobsson, M., Jordan, T. M., Kjeldsen, K. K., Millan, R., Mayer, L., Mouginot, J., Noël, B. P. Y., O’Cofaigh, C., Palmer, S., Rysgaard, S., Seroussi, H., Siegert, M. J., Slabon, P., Straneo, F., van den Broeke, M. R., Weinrebe, W., Wood, M., and Zinglensen, K. B.: BedMachine v3: Complete Bed Topography and Ocean Bathymetry Mapping of Greenland From Multibeam Echo Sounding Combined With Mass Conservation, *Geophysical Research Letters*, 44, 11,051–11,061, <https://doi.org/10.1002/2017GL074954>, 2017.
- Mullen, S. L.: The Impact of Orography on Blocking Frequency in a General Circulation Model, *Journal of Climate*, 2, 1554–1560, [https://doi.org/10.1175/1520-0442\(1989\)002<1554:TIOOOB>2.0.CO;2](https://doi.org/10.1175/1520-0442(1989)002<1554:TIOOOB>2.0.CO;2), 1989.
- Muntjewerf, L., Petrini, M., Vizcaíno, M., Ernani da Silva, C., Sellevold, R., Scherrenberg, M. D. W., Thayer-Calder, K., Bradley, S. L., Lenaerts, J. T. M., Lipscomb, W. H., and Lofverstrom, M.: Greenland Ice Sheet Contribution to 21st Century Sea Level Rise as Simulated by the Coupled CESM2.1-CISM2.1, *Geophysical Research Letters*, 47, e2019GL086836, <https://doi.org/10.1029/2019GL086836>, 2020a.
- 595 Muntjewerf, L., Sellevold, R., Vizcaíno, M., Ernani da Silva, C., Petrini, M., Thayer-Calder, K., Scherrenberg, M. D. W., Bradley, S. L., Katsman, C. A., Fyke, J., Lipscomb, W. H., Lofverstrom, M., and Sacks, W. J.: Accelerated Greenland Ice Sheet Mass Loss Under High Greenhouse Gas Forcing as Simulated by the Coupled CESM2.1-CISM2.1, *Journal of Advances in Modeling Earth Systems*, 12, e2019MS002031, <https://doi.org/10.1029/2019MS002031>, 2020b.
- 600 Muntjewerf, L., Sacks, W. J., Lofverstrom, M., Fyke, J., Lipscomb, W. H., Ernani da Silva, C., Vizcaíno, M., Thayer-Calder, K., Lenaerts, J. T. M., and Sellevold, R.: Description and Demonstration of the Coupled Community Earth System Model v2 – Community Ice Sheet Model v2 (CESM2-CISM2), *Journal of Advances in Modeling Earth Systems*, 13, <https://doi.org/10.1029/2020MS002356>, 2021.
- Narinesingh, V., Booth, J. F., Clark, S. K., and Ming, Y.: Atmospheric Blocking: The Impact of Topography in an Idealized General Circulation Model, *Weather and Climate Dynamics Discussions*, <https://doi.org/10.5194/wcd-2020-2>, 2020.
- 605 Notz, D.: The future of ice sheets and sea ice: Between reversible retreat and unstoppable loss, *Proceedings of the National Academy of Sciences*, 106, 20590–20595, <https://doi.org/10.1073/pnas.0902356106>, 2009.
- Notz, D. and Stroeve, J.: Observed Arctic sea-ice loss directly follows anthropogenic CO₂ emission, *Science*, 354, 747–750, <https://doi.org/10.1126/science.aag2345>, 2016.
- 610 Noël, B., Lenaerts, J. T. M., Lipscomb, W. H., Thayer-Calder, K., and van den Broeke, M. R.: Peak refreezing in the Greenland firn layer under future warming scenarios, *Nature Communications*, 13, 6870, <https://doi.org/10.1038/s41467-022-34524-x>, 2022.
- Oh, J.-H., An, S.-I., Shin, J., and Kug, J.-S.: Centennial Memory of the Arctic Ocean for Future Arctic Climate Recovery in Response to a Carbon Dioxide Removal, *Earth’s Future*, 10, e2022EF002804, <https://doi.org/10.1029/2022EF002804>, 2022.
- Otosaka, I. N., Shepherd, A., Ivins, E. R., Schlegel, N.-J., Amory, C., van den Broeke, M. R., Horwath, M., Joughin, I., King, M. D., Krinner, G., Nowicki, S., Payne, A. J., Rignot, E., Scambos, T., Simon, K. M., Smith, B. E., Sørensen, L. S., Velicogna, I., Whitehouse, P. L., Agosta, C., Ahlstrøm, A. P., Blazquez, A., Colgan, W., Engdahl, M. E., Fettweis, X., Forsberg, R., Gallée, H., Gardner, A., Gilbert, L., Gourmelen, N., Groh, A., Gunter, B. C., Harig, C., Helm, V., Khan, S. A., Kittel, C., Konrad, H., Langen, P. L., Lecavalier, B. S., Liang, C.-C., Loomis, B. D., McMillan, M., Melini, D., Mernild, S. H., Mottram, R., Mouginot, J., Nilsson, J., Noël, B., Pattle, M. E., Peltier, W. R., Pie, N., Roca, M., Sasgen, I., Save, H. V., Seo, K.-W., Scheuchl, B., Schrama, E. J. O., Schröder, L., Simonsen, S. B., Slater, T., Spada, G.,

- 620 Sutterley, T. C., Vishwakarma, B. D., van Wessem, J. M., Wiese, D., van der Wal, W., and Wouters, B.: Mass balance of the Greenland and Antarctic ice sheets from 1992 to 2020, *Earth System Science Data*, 15, 1597–1616, <https://doi.org/10.5194/essd-15-1597-2023>, 2023.
- Pall, P., Allen, M. R., and Stone, D. A.: Testing the Clausius–Clapeyron constraint on changes in extreme precipitation under CO₂ warming, *Climate Dynamics*, 28, 351–363, <https://doi.org/10.1007/s00382-006-0180-2>, 2007.
- Pattyn, F., Ritz, C., Hanna, E., Asay-Davis, X., DeConto, R., Durand, G., Favier, L., Fettweis, X., Goelzer, H., Gollledge, N. R.,
625 Kuipers Munneke, P., Lenaerts, J. T. M., Nowicki, S., Payne, A. J., Robinson, A., Seroussi, H., Trusel, L. D., and van den Broeke, M.: The Greenland and Antarctic ice sheets under 1.5 °C global warming, *Nature Climate Change*, 8, 1053–1061, <https://doi.org/10.1038/s41558-018-0305-8>, 2018.
- Reynolds, C. A., Crawford, W., Huang, A., Barton, N., Janiga, M. A., McLay, J., Flatau, M., Frolov, S., and Rowley, C.: Analysis of Integrated Vapor Transport Biases, *Monthly Weather Review*, 150, 1097–1113, <https://doi.org/10.1175/MWR-D-21-0198.1>, 2022.
- 630 Ribes, A. and Terray, L.: Application of regularised optimal fingerprinting to attribution. Part II: Application to global near-surface temperature, *Climate Dynamics*, 41, <https://doi.org/10.1007/s00382-013-1736-6>, 2013.
- Ridley, J., Gregory, J. M., Huybrechts, P., and Lowe, J.: Thresholds for irreversible decline of the Greenland ice sheet, *Climate Dynamics*, 35, 1049–1057, <https://doi.org/10.1007/s00382-009-0646-0>, 2010.
- Ridley, J. K., Huybrechts, P., Gregory, J. M., and Lowe, J. A.: Elimination of the Greenland Ice Sheet in a High CO₂ Climate, *Journal of*
635 *Climate*, 18, 3409–3427, <https://doi.org/10.1175/JCLI3482.1>, 2005.
- Robinson, A., Calov, R., and Ganopolski, A.: Multistability and critical thresholds of the Greenland ice sheet, *Nature Climate Change*, 2, 429–432, <https://doi.org/10.1038/nclimate1449>, 2012.
- Sellevold, R. and Vizcaíno, M.: Global Warming Threshold and Mechanisms for Accelerated Greenland Ice Sheet Surface Mass Loss, *Journal of Advances in Modeling Earth Systems*, 12, e2019MS002029, <https://doi.org/10.1029/2019MS002029>, 2020.
- 640 Sellevold, R., van Kampenhout, L., Lenaerts, J. T. M., Noël, B., Lipscomb, W. H., and Vizcaíno, M.: Surface mass balance downscaling through elevation classes in an Earth System Model: analysis, evaluation and impacts on the simulated climate, *The Cryosphere Discussions*, <https://doi.org/10.5194/tc-2019-122>, 2019.
- Sellevold, R., Lenaerts, J. T. M., and Vizcaíno, M.: Influence of Arctic sea-ice loss on the Greenland ice sheet climate, *Climate Dynamics*, 58, 179–193, <https://doi.org/10.1007/s00382-021-05897-4>, 2022.
- 645 Smith, M. M., Holland, M., and Light, B.: Arctic sea ice sensitivity to lateral melting representation in a coupled climate model, *The Cryosphere*, 16, 419–434, <https://doi.org/10.5194/tc-16-419-2022>, 2022.
- Smith, R., Jones, P., Briegleb, B., Bryan, F., Danabasoglu, G., Dennis, J., Dukowicz, J., Eden, C., Fox-Kemper, B., Gent, P., Hecht, M., Jayne, S., Jochum, M., Large, W., Lindsay, K., Maltrud, M., Norton, N., Peacock, S., Vertenstein, M., and Yeager, S.: The Parallel Ocean Program (POP) Reference Manual, <http://n2t.net/ark:/85065/d70g3j4h>, 2010.
- 650 Swingedouw, D., Houssais, M.-N., Herbaut, C., Blaizot, A.-C., Devilliers, M., and Deshayes, J.: AMOC Recent and Future Trends: A Crucial Role for Oceanic Resolution and Greenland Melting?, *Frontiers in Climate*, 4, <https://doi.org/10.3389/fclim.2022.838310>, 2022.
- Sévellec, F., Fedorov, A. V., and Liu, W.: Arctic sea-ice decline weakens the Atlantic Meridional Overturning Circulation, *Nature Climate Change*, 7, 604–610, <https://doi.org/10.1038/nclimate3353>, 2017.
- Vizcaíno, M.: Ice sheets as interactive components of Earth System Models: progress and challenges, *WIREs Climate Change*, 5, <https://doi.org/10.1002/wcc.285>, 2014.
- 655 Vizcaíno, M., Mikolajewicz, U., Gröger, M., Maier-Reimer, E., Schurgers, G., and Winguth, A. M. E.: Long-term ice sheet–climate interactions under anthropogenic greenhouse forcing simulated with a complex Earth System Model, *Climate Dynamics*, 31, 665–690, <https://doi.org/10.1007/s00382-008-0369-7>, 2008.
- Vizcaíno, M., Mikolajewicz, U., Ziemann, F., Rodehacke, C. B., Greve, R., and van den Broeke, M. R.: Coupled simulations of Greenland Ice
660 Sheet and climate change up to A.D. 2300, *Geophysical Research Letters*, 42, 3927–3935, <https://doi.org/10.1002/2014GL061142>, 2015.
- Wu, P., Jackson, L., Pardaens, A., and Schaller, N.: Extended warming of the northern high latitudes due to an overshoot of the Atlantic meridional overturning circulation, *Geophysical Research Letters*, 38, <https://doi.org/10.1029/2011GL049998>, 2011.
- Zeitz, M., Haacker, J. M., Donges, J. F., Albrecht, T., and Winkelmann, R.: Dynamic regimes of the Greenland Ice Sheet emerging from interacting melt–elevation and glacial isostatic adjustment feedbacks, *Earth System Dynamics*, 13, 1077–1096, <https://doi.org/10.5194/esd-13-1077-2022>, 2022.
- 665

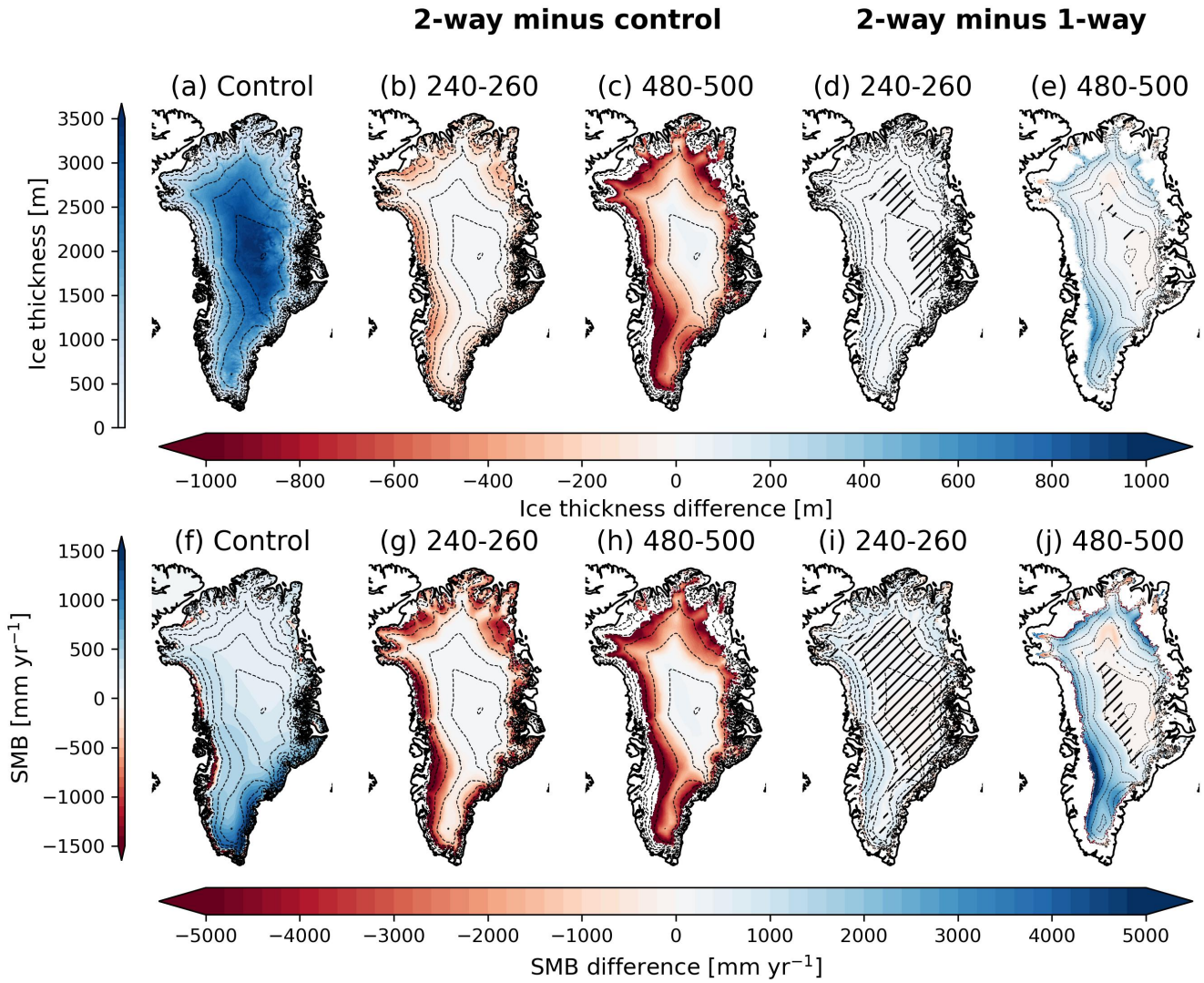


Figure A1. Ice thickness [m] and surface mass balance (SMB) [mm yr^{-1}] as downscaled to the CISM2 grid (4 km) for (a, f) the mean of the control simulation, (b, c, g, h) anomalies of the 2-way coupled simulation with respect to the control simulation and (d, e, i, j) anomalies of the 2-way with respect to the 1-way coupled simulation for grid points that have not deglaciated in both simulations, for (b, d, g, i) the years 240-260 and (c, e, h, j) the years 480-500. The dashed black lines depict contour lines for every 500 m elevation of the control (a, f) and 2-way coupled (b-e, g-j) simulations. Hatches denote areas in which the differences between the 1- and 2-way coupled simulations have not become significant before the last year of the corresponding period. Because of a different evolution of ice sheet topography, the two simulations show a different SMB pattern, leading to a few locations in which the 1-way simulation shows less SMB reduction.

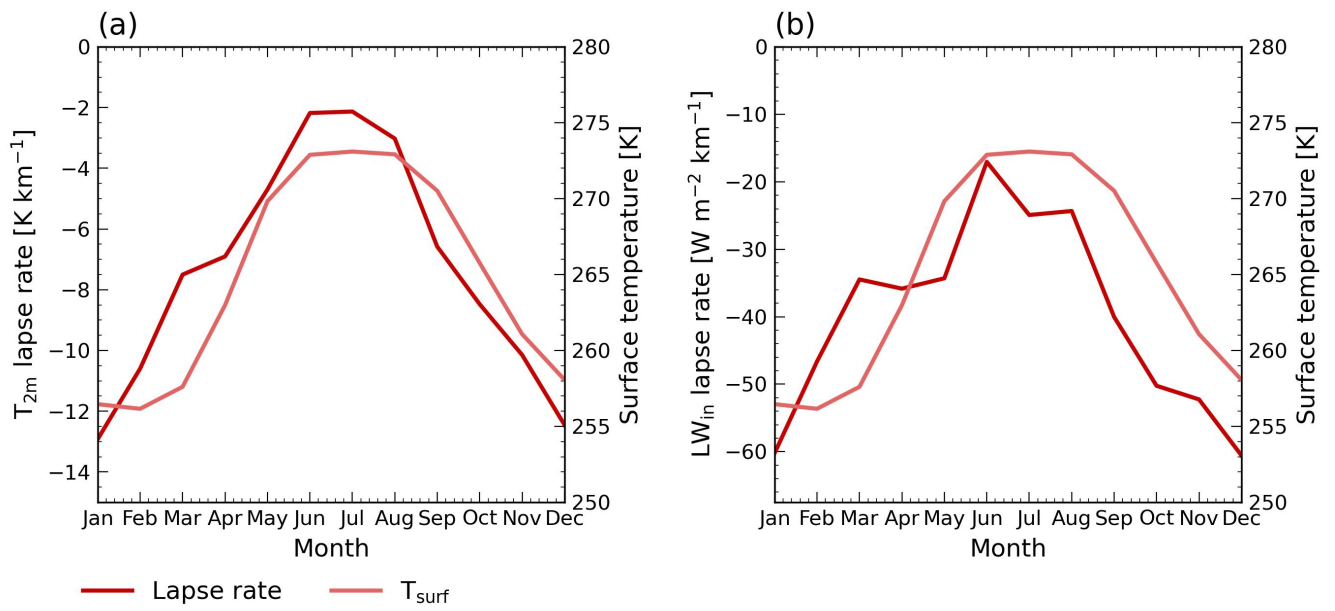


Figure A2. Monthly lapse rates (dark red) for (a) 2m air temperature [$K km^{-1}$] and (b) incoming longwave radiation [$W m^{-2} km^{-1}$] for years 480-500. The light red line shows the monthly mean surface temperature [K] of the locations considered for computing the lapse rates and is the same in both (a) and (b).

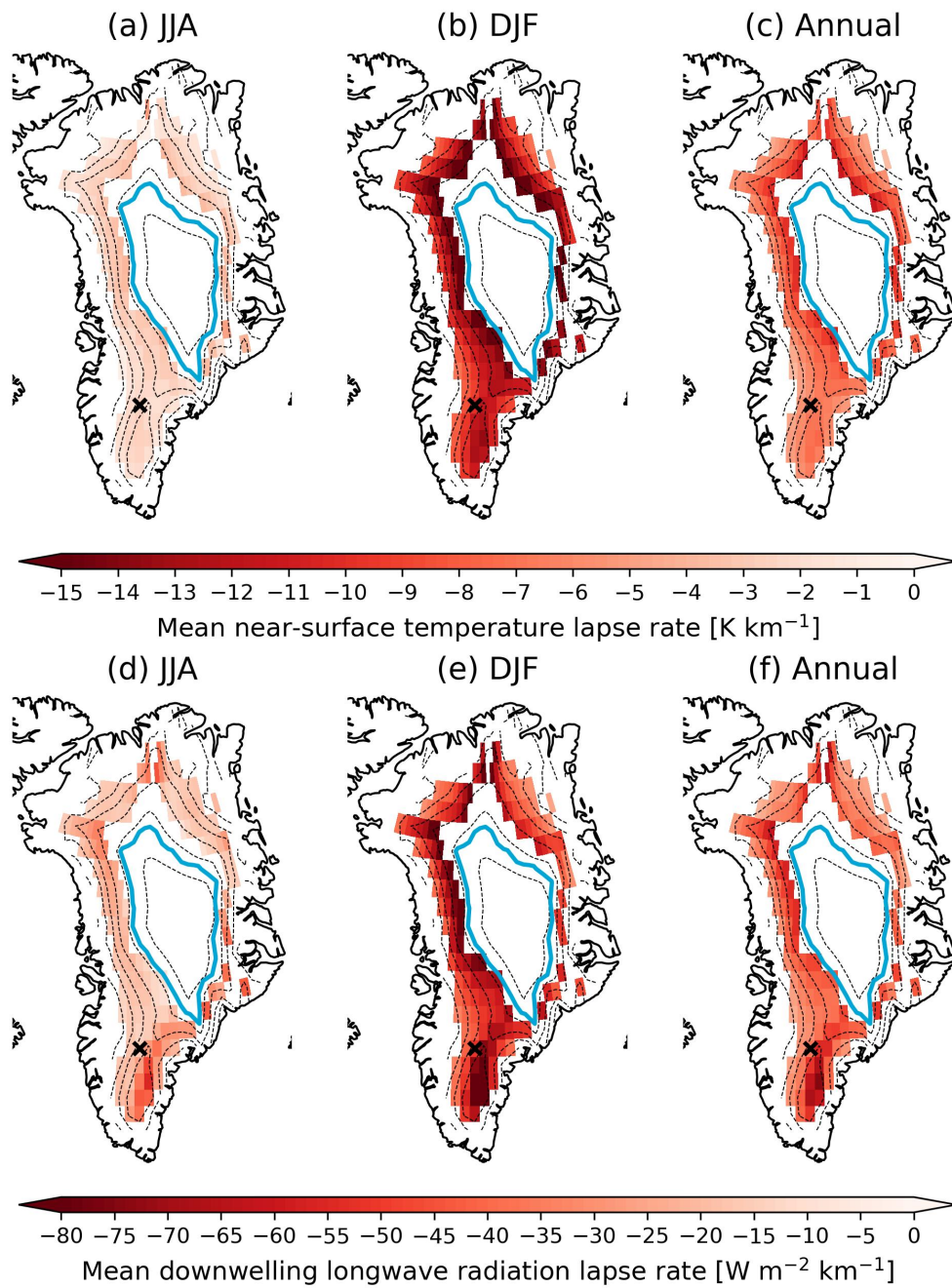


Figure A3. Lapse rate of (a-c) near-surface (2 m) air temperature [K km^{-1}] and (d-f) downwelling shortwave radiation [$\text{W m}^{-2} \text{km}^{-1}$] for (a, d) June, July, August (JJA) mean, (b, e) December, January, February (DJF) mean and (c, f) annual mean. The black lines depict contour lines for every 500 m elevation of the 2-way simulation. The light blue line represents the ELA of the 2-way simulation. The black cross shows the location of the point shown in Figure 5.

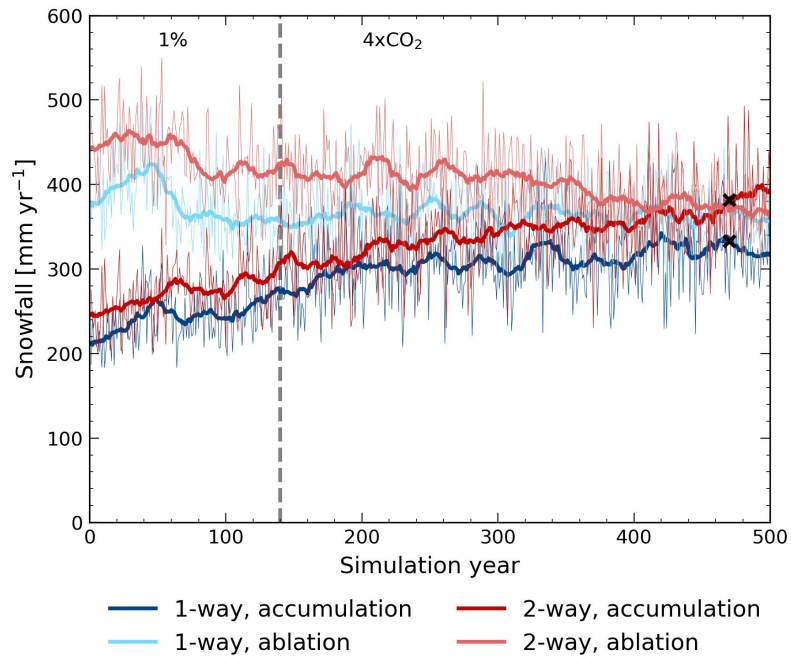


Figure A4. Evolution of snowfall [mm yr^{-1}] in the 1-way (blue) and 2-way (red) coupled simulation for the end-of-simulation ablation and accumulation area. The grey dashed line indicates the end of the 1 % CO_2 ramp-up period and the start of the continuous 4xCO_2 period. If the differences between the 1- and 2-way coupled simulations become significant throughout the simulation, the first year of significant difference is marked with a black cross.

Table A1. Year of recovery. In case the variable has not recovered by the end of the simulation (year 925), the remaining anomaly of the mean state of the variable in the last 100 years of the simulation with respect to the closest boundary of the $1\text{-}\sigma$ confidence interval is computed, as well as the remaining linear trend over the last 100 years. A positive anomaly means that the end-of-simulation state of the variable is larger than in the control simulation. If the trend and remaining anomaly are in the opposite direction, an extrapolated recovery year is given. The relative amount of recovery [%] is given for variables that have not recovered by the end of the simulation.

	Year of recovery	Remaining anomaly	Remaining trend	Extrapolated year of recovery	Percentage recovered
Mean global T_{2m}	-	1.94 K	$-0.00022 \text{ K yr}^{-1}$	9567	76 %
Mean GrIS T_{2m}	-	2.30 K	$-0.0099 \text{ K yr}^{-1}$	1157	68 %
Mean Arctic T_{2m}	-	3.71 K	0.0017 K yr^{-1}	-	70 %
Total mass balance	452	-	-	-	-
Surface mass balance	-	-339 Gt yr^{-1}	-0.23 Gt yr^{-2}	-	89 %
Calving flux	-	-444 Gt yr^{-1}	$-0.088 \text{ Gt yr}^{-2}$	-	16 %
March sea ice extent	-	$-1.04 \cdot 10^6 \text{ km}^2$	$0.00076 \cdot 10^6 \text{ km}^2 \text{ yr}^{-1}$	2291	90 %
September sea ice extent	-	$-5.39 \cdot 10^6 \text{ km}^2$	$-0.00092 \cdot 10^6 \text{ km}^2 \text{ yr}^{-1}$	-	14 %
March sea ice thickness	-	-0.64 m	$-0.00047 \text{ m yr}^{-1}$	-	55 %
September sea ice thickness	-	-0.74 m	$-0.000099 \text{ m yr}^{-1}$	-	9 %
NAMOC index	-	4.84 Sv	$-0.0062 \text{ Sv yr}^{-1}$	1707	-
Labrador Sea MLD	-	115.5 m	0.80 m yr^{-1}	-	-
Irminger Sea MLD	700	-	-	-	-
Norwegian Sea MLD	459	-	-	-	-
Nansen Basin MLD	915	-	-	-	-
Refreezing capacity	-	-0.08	0.000024 yr^{-1}	4352	62 %

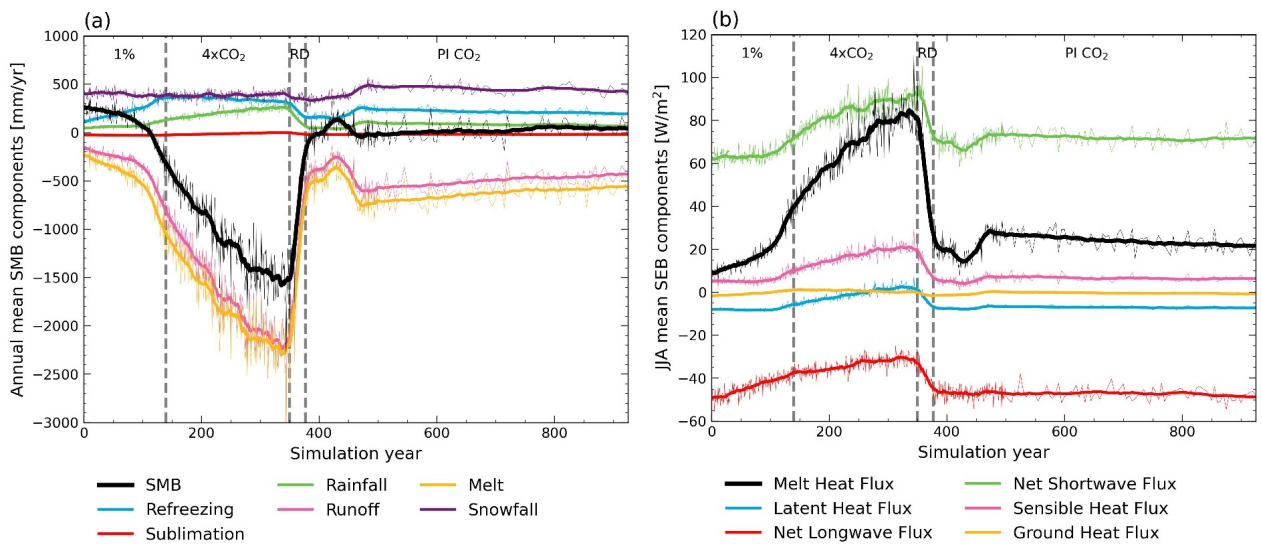


Figure A5. Evolution of (a) GrIS annual mean SMB [mm yr^{-1}] and its components and (b) GrIS JJA (June, July, August) mean SEB [W m^{-2}] and its components for the simulation in which we reintroduce PI CO_2 . The grey dashed lines indicate the end of the 1% CO_2 ramp-up, the continuous $4\times\text{CO}_2$, the ramp-down (RD) to PI CO_2 and the continuous PI CO_2 periods.

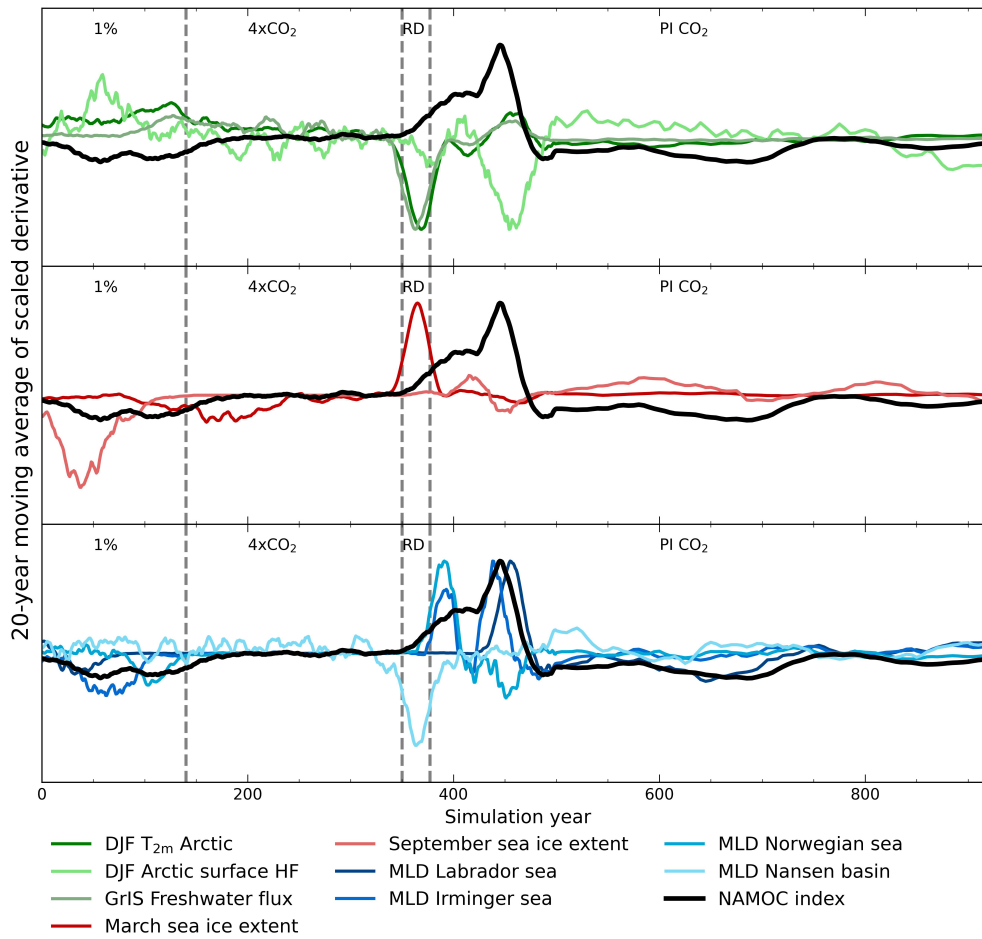


Figure A6. 20-year moving average of the derivative of processes interacting with the NAMOC (black). These are the winter Arctic T_{2m} , the winter Arctic surface heat flux, the GrIS freshwater flux, the March and September sea ice extent, and the winter MLDs in the Labrador Sea, Irminger Sea, Norwegian Sea, and Nansen Basin. The derivatives are computed using the central difference method and thereafter scaled to their maximum response. The grey dashed lines indicate the end of the 1 % CO_2 ramp-up, the continuous $4xCO_2$, the ramp-down (RD) to PI CO_2 and the continuous PI CO_2 periods.

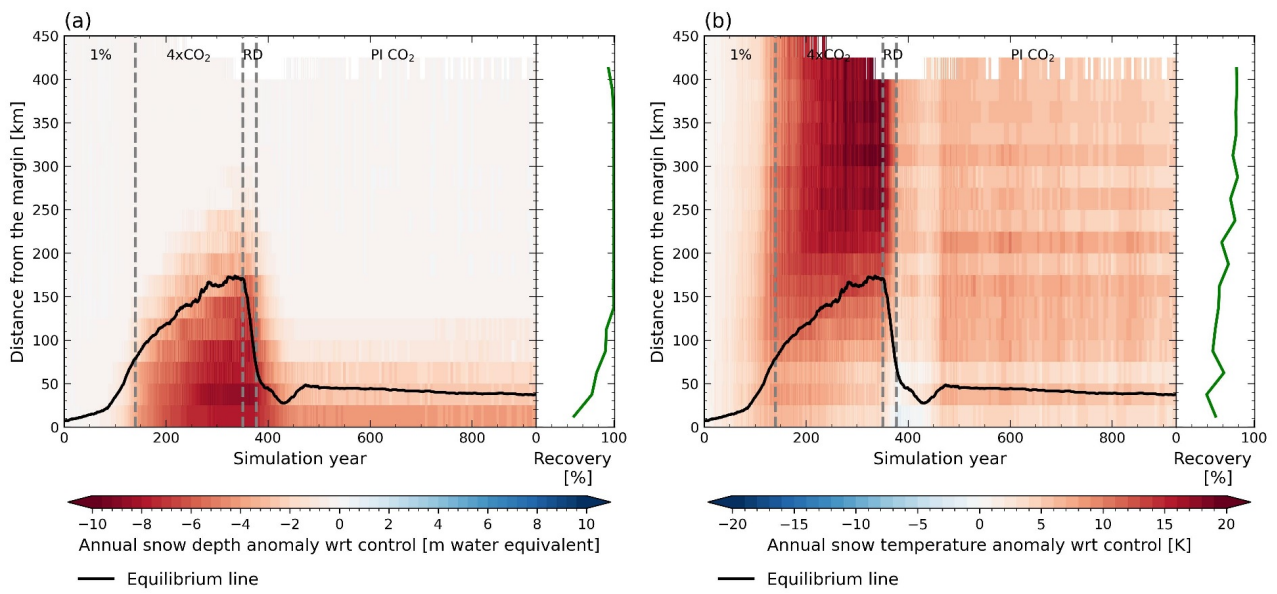


Figure A7. Anomalies of (a) annual mean snow depth [m water equivalent] and b) the annual mean snow temperature [K] over the GrIS with respect to the control mean as a function of time and distance to the ice sheet margin for the reintroduction of PI CO₂ simulation. The black line denotes the mean distance of the equilibrium line to the margin and the dark green line shows the relative recovery (in %) for each distance class. The grey dashed lines indicate the end of the 1 % CO₂ ramp-up, the continuous 4xCO₂, the ramp-down (RD) to PI CO₂ and the continuous PI CO₂ periods.

Appendix B: Interactions and feedbacks between the Greenland ice sheet and Earth system

In this section, we discuss the different interactions and feedback mechanisms that influence and interact with the GrIS mass balance and the climate in the Arctic, North Atlantic, and over the GrIS. These interactions can be accounted for in a coupled Earth system-ice sheet model and can influence climate and SLR projections. We first consider GrIS feedback mechanisms, related to mass loss. Then we look into feedbacks and interactions with the atmosphere and ocean and consider interactions with Arctic sea ice changes.

The GrIS surface processes are affected by a changing climate, and in turn, these changes influence the climate as well through interactions and feedbacks between the GrIS and Earth system (Vizcaíno, 2014; Fyke et al., 2018). These interactions can lead to an amplified response, moving the system further away from its equilibrium state, which is known as a positive feedback. Positive feedback mechanisms can accelerate GrIS melt processes, potentially triggering tipping points. When a tipping point threshold is crossed, the ice sheet may not be able to regain its initial state, resulting in complete or near-complete loss of the ice sheet (Pattyn et al., 2018; Gregory et al., 2020). On the other hand, when a negative feedback occurs, the response of a system to the forcing is dampened, pushing the system back to its equilibrium state. Therefore, negative feedback mechanisms have the potential to slow down GrIS mass loss.

One of the most important GrIS feedback mechanisms occurring is the positive melt-elevation feedback. When a forcing related to ablation (accumulation), such as an increase (decrease) in summer air temperature, occurs, the melt will increase (decrease), leading to a lowering (heightening) of the GrIS elevation. As the temperature is higher (lower) at lower (higher) elevations, this results in enhanced (decreased) melt (Fyke et al., 2018). The melt-elevation feedback can play an important role over multi-centennial timescales, particularly under higher emission scenarios (Edwards et al., 2014; Vizcaíno, 2014). Another important positive feedback mechanism is the melt-albedo feedback (Box et al., 2012). Similar to the melt-elevation feedback, an ablation-related forcing can lead to increased melt. Fresh snow has a high albedo, reflecting a large fraction of the incoming solar radiation. However, snow melt leads to a reduction of the surface albedo, resulting in less solar radiation being reflected, which adds to the energy available for melting, thereby enhancing melt processes. As these positive feedback mechanisms both come into play during summer melt conditions, they can enhance each other's melt responses, resulting in an acceleration of the subsequent melting (Fyke et al., 2018).

Negative feedback mechanisms related to a changing GrIS geometry can stabilize GrIS melt processes. As ice sheet melting occurs, the ablation area will shrink as a result of the melting process, resulting in a smaller area in which melt occurs, stabilizing the melting process (Fyke et al., 2018). Next to that, a changing geometry has the potential to change atmospheric circulation and could therefore change precipitation patterns. As the surface lowers, moisture will be able to advect further landwards, resulting in a decrease in precipitation in coastal regions and an increase in precipitation around the interior. Besides, as the ice sheet advances inwards, downslope katabatic winds could potentially cool the margins (Ridley et al., 2005), acting as a negative feedback. Another negative feedback mechanism is the melt-discharge feedback (Goelzer et al., 2013; Fürst et al., 2015; Vizcaíno et al., 2015). As the ice sheet melts, the margins will thin and retreat landward. As ice thickness is reduced, the gravitational stress at the grounding line reduces, resulting in a smaller discharge. In case the grounding line retreats from marine to terrestrial, the local discharge even reduces to zero. These mechanisms result in a smaller discharge and therefore smaller overall ice mass loss when melting becomes stronger.

Besides ice sheet-atmosphere feedbacks, feedbacks between the ice sheet and the ocean can emerge as well. Outlet glaciers are influenced by ocean dynamics and can influence ice dynamics as they retreat. However, since there is a limited number of outlet glaciers present around the GrIS, these interactions do not play a significant role, in contrast to the AIS, which consists of a large number of ice shelves. However, of importance to the evolution of the GrIS is the evolution of the North Atlantic Meridional Overturning Circulation (NAMOC). The NAMOC is the Northern branch of the Atlantic Meridional Overturning Circulation (AMOC) and is a density-driven circulation. Density gradients in the Atlantic arise from temperature and salinity gradients, because of which the AMOC is referred to as a thermohaline circulation. Warmer surface waters, which have a lower density, are transported to the colder high latitudes as a result of a latitudinal ocean water density gradient. During winter, the atmosphere cools these surface waters, which increases their density. This increase in density causes the surface waters to

sink at high latitudes, forming the North Atlantic deep waters (NADW) in the Nordic seas and the Labrador sea (Swingedouw et al., 2022). The vertical transport of cold water to the deeper ocean and its replacement at the surface with warmer waters coming from the south is called overturning. A high salinity at high latitudes is a prerequisite for overturning, as saline waters are denser, enhancing the downwelling of cooled surface waters (Blanke et al., 2006). The depth of these downwelling ocean waters (referred to as the mixed layer depth (MLD)) largely determines the strength of the AMOC (Bretones et al., 2022). The MLD is largest in winter, as there is a large ocean surface heat flux between the warm ocean and cold atmosphere, which destabilizes the upper ocean and leads to enhanced mixing and therefore larger MLDs (Bretones et al., 2022). Therefore, stronger winter cooling leads to enhanced NAMOC strength (Kostov et al., 2019). Besides, Arctic sea ice grows in winter and melts in summer, which affects the density, and thus on the overturning in high latitudes. As sea ice melts, freshwater is released into the ocean, leading to lower salinity and therefore smaller density gradients, reducing the overturning. In winter, the opposite is the case, as Arctic sea ice regrows. As the salt water freezes, the salt will be pushed out, which is called brine rejection. This causes the surrounding water to become more saline, and therefore denser, enhancing the overturning (Marshall and Plumb, 2008). As the NAMOC is responsible for a large part of the northward ocean heat transport, it has a large influence on GrIS temperatures. However, the GrIS itself influences the NAMOC as well. An increase in North Atlantic freshwater fluxes due to increased melt has the potential to slow down the NAMOC (Vizcaíno et al., 2008), as it reduces the salinity of the surrounding waters, resulting in a lower density, diminishing the formation of NADW. A slowdown of the NAMOC leads to smaller northward heat transport and can therefore result in a cooling effect in the North Atlantic, which slows down GrIS mass loss (Vizcaíno et al., 2008). Therefore, the interaction between the NAMOC and the GrIS can be considered a negative feedback.

In a warming climate, not only the GrIS and AIS will lose ice mass, but the Arctic sea ice extent is projected to decline as well. Notz and Stroeve (2016) showed that the loss of Arctic sea ice scales linearly with both global temperature and cumulative CO₂ emissions. As sea ice melts and the Arctic sea ice extent decreases, the sea ice loss will be amplified by the sea ice-albedo feedback, as less solar radiation is reflected, resulting in larger surface temperatures, which enhances melt (Curry et al., 1995). Open-water formation in the Arctic, driven by the sea ice-albedo feedback, can result in thinner ice and a decrease in sea ice extent as ocean temperatures increase due to larger absorption of shortwave radiation (Smith et al., 2022). Sellevold et al. (2022) showed that a decrease in Arctic sea ice can result in enhanced winter precipitation over the GrIS, as well as enhanced melt in summer, due to atmospheric circulation changes and increases in turbulent fluxes. Similarly, Liu et al. (2016) showed that increased GrIS summer melt is linked to Arctic sea ice loss through changes in atmospheric circulation and an increase in incoming longwave radiation. These studies show that Arctic sea ice decline as a result of global warming has the potential to enhance GrIS mass loss. Besides, a changing Arctic can affect the evolution of the GrIS by influencing the NAMOC. The overturning at high latitudes is driven by density differences. As Arctic sea ice melt increases in summer and sea ice regrowth reduces in winter, the surrounding waters will become fresher, which reduces the overturning and can therefore weaken the NAMOC, reducing heat transport into the Arctic (Sévellec et al., 2017). This not only influences the GrIS temperatures but can lower Arctic temperatures as well, which can slow down the loss of Arctic sea ice.